A sensitivity analysis of acoustic wave propagation through the ankle joint space.

Roos Marieke Oosting

Delft University of Technology

TU Delft

A sensitivity analysis of acoustic wave propagation through the ankle joint space.

By

Roos Marieke Oosting

in partial fulfilment of the requirements for the degree of

Master of Science

in Biomedical engineering

at the Delft University of Technology,

to be defended on Friday January 15, 2016 at 9:30 AM.

Supervisors: M. Stijntjes MSc, Dr.ir. G.J.M. Tuijthof, Prof.dr.J. Dankelman

This thesis is confidential and cannot be made public until December 31, 2018.

Introduction thesis

Sport or in-house trauma result in 1 million people yearly in cartilage damage, lesions involving articular cartilage and its subchondral bone are called osteochondral defects (OCDs). Currently used imaging techniques that are used for the detection of OCDs are invasive and costly. Decision making for treatment is highly driven by the defect size, it would therefore by favourable to detect OCDs as early as possible, this limits the risks of treatment. A diagnostic technique in which acoustic wave propagation through the entire joint space is used for the detection of OCDs is therefore investigated. The proposed diagnostic technique is developed for a broad range of people. The relation between acoustic wave propagation and acoustic parameters of bone should therefore be studied. The starting point of this thesis were the simulations of acoustic wave propagation through the ankle joint performed by Nazli Sarkalkan (PhD, Biomedical engineering, TU Delft). Simulations were performed on a simplified model of the ankle joint. This thesis aims to generate a more complete model of the ankle joint space with acoustic parameters of bone and the presence of soft tissues. A literature study was performed for the acoustic parameters of bone. The variation in the acoustic parameters that was found was assumed to be a good starting point to investigate the sensitivity of acoustic wave propagation to the natural variation in acoustic parameters of bone. Limited information of the acoustic parameters of Achilles tendon and skin was found in literature. To elaborate the computational model of the ankle joint space with Achilles tendon and skin an experiment was conducted. Appendix A describes the dissection of 11 human cadaver ankles of which the Achilles tendon, skin and other soft tissues were dissected. The main interest of our study was on skin and Achilles tendon because we assumed that these tissues were a good starting point to elaborate the model of the ankle joint space with soft tissues. The presence of skin and Achilles tendon were used to indicate whether acoustic wave propagation is sensitive to the presence of soft tissues. The acoustic parameters of Achilles tendon and skin were determined by the use of the Marco scanner and the density bottle method. The Macro scanner was built by Lana Keijzer (Msc. Applied physics, TU Delft) and Dr. Koen W.A van Dongen (Applied physics, TU Delft). The set-ups and the experiments that were performed are described in Appendix B. The data processing steps that are conducted are described in Appendix C. The acoustic parameters of the extensor digitorum longus and peroneus brevus are presented in Appendix D. Although these tissues were not used in this model of the ankle joint space it is expected that the acoustic parameter values can be of interest in future studies that will be performed to investigate the feasibility of the proposed diagnostic technique. The article describes the results of the sensitivity analysis extensively however Appendix E gives a graphical presentation of the creation of the geometry, acoustic wave propagation through the ankle joint space and the output signals.

Table of contents

A sensitivity analysis to assess the influence of variation in acoustic parameters of bone and the presence of soft tissues on acoustic wave propagation and the identification of osteochondral defects within the ankle joint space.

R.M. Oosting, M. Stijntjes MSc, Dr.ir. G.J.M. Tuijthof, Prof.dr.J. Dankelman

Abstract

Ultrasound imaging is known to be non-invasive, fast, and cost-effective. However, a drawback is its reflection on bone. Therefore, an alternative acoustic wave propagating technique is being developed that eventually should be able to diagnose osteochondral defects (OCDs) that are now often missed with conventional imaging techniques. A novel technique is proposed that consists of acoustic wave propagation through the ankle joint space. The identification of OCDs is based on a presumed deviation between a reference signal (from a predicted model of the patient specific healthy ankle joint space) and a measured signal including the OCD in de ankle joint space. For the identification of OCDs, the diagnostic technique should be robust enough to cope with variation in acoustic parameters. To assess the influence of acoustic parameters, two dimensional finite-difference time-domain models of the ankle joint space were generated.
A sensitivity analysis was performed to indicate the effect of variation in acoustic parameters of bone, the presence of soft tissues on acoustic wave propagation and the identification of OCDs. The minimal, maximal and mean values of the density, the Lamé's constants, shear and bulk viscosity of bone were variated step by step. The values of acoustic bone parameters were derived from literature, those of the Achilles tendon and skin were determined experimentally. The output signals from the receiver that was placed on the outside of the ankle joint space were of main interest during present study. The output signals of the receiver in the middle and the anterior side of the ankle joint space were assessed to gain more insight in the behaviour of the acoustic waves within the ankle joint space. Variation in acoustic parameters of bone made noticeable alterations to the reference signal: variation in density resulted in normalized root mean square error (NRMSE) from 10%-16%, variation in the Lamé's constants resulted in NRMSE from 8% -13% and variation in the bulk and shear viscosity ranged from 6% -10%. In comparison the NRMSE as a result of an OCD of 5 mm wide and 5 mm deep in the middle of the talus ranged from 5% to 7%. The receiver that was placed in the middle of the ankle joint space showed larger differences in amplitude and time shift between the healthy and defected ankle condition. The NRMSE caused by the variation in acoustic parameters of bone ranged from 1% - 10%, whereas the NRMSE caused by the presence of an OCD ranged from 10%-12%. The detectability of an OCD increases with the presence of Achilles tendon and skin. A slight difference in NRMSE and NMCC, the missing time shift and the least influence on the amplitude by the bulk and shear viscosity implies that acoustic wave propagation is less sensitive to variation in the shear and bulk viscosity than in density and Lamé's constants. It is advised that the acoustic parameters of bone and soft tissues are estimated precisely when models of the ankle joint space for OCD identification purposes are developed.

Keywords: *osteochondral defects; ankle joint; ankle joint space; ultrasound propagation; two dimensional finite-difference time-domain model; sensitivity analysis; pulse echo method; density bottle method*

Introduction

Yearly 15 million people suffer from in-house and sports traumas. In one million people this results in cartilage damage which is characterized by a fissure or by an increase in stiffness (1, 2). Lesions involving articular cartilage and its subchondral bone are called osteochondral defects (OCDs). OCDs can heal and remain asymptomatic. However, without treatment they can lead to deep ankle pain, joint swelling, and limited range of motion. Untreated OCDs have the potential to develop into early osteoarthritis (OA) (3, 4). Decision making for treatment of OCDs is largely dependent on the size of the OCDs; small OCDs can be treated by the use of a brace, while large OCDs need to be treated by a minimal invasive surgery. During this surgery the defected cartilage is removed, and small holes in the underlying bones are made to enhance the blood flow. Cartilage tissue will regrow in a few months. Diagnosis of OCDs in an early stage is favoured because the large OCDs increase the risks of treatment. Additionally, early diagnosis will reduce the development of early OA. Computed tomography (CT) and magnetic resonance imaging (MRI) are currently used to diagnose OCDs. These techniques are sensitive in identification of OCDs, but CT requires a contrast agent for the identification of small OCDs (5) whereas it is challenging to read the size of an OCD from images obtained with MRI. The classification of the size of OCDs tends to be overrated when read from MRI images(6). Moreover, these techniques are costly, CT uses ionizing radiation and MRI has a long acquisition time. A manageable device which can adequately indicate cartilage damage and which can be used outside the clinic would be preferred. Conventional ultrasound imaging is known to be non-invasive, fast, and cost-effective (7) but not capable of imaging most cartilage OCDs (8) because acoustic waves are highly attenuated when penetrated through bone (9).

A diagnostic technique in which acoustic waves are used in a different setting which enables the screening of the entire ankle joint space without the need to penetrate bone is therefore proposed in literature (10-12). The proposed novel diagnostic technique is based on the definition that the output signal of an ankle joint space with an OCD deviates from a reference signal (that is associated with a healthy ankle joint space) caused by the presence of an OCD. For successful identifications of OCDs, the diagnostic technique should be robust enough to cope with variation in acoustic parameters of bone and presence of soft tissues. However, currently little is known about acoustic wave propagation through the ankle joint space and the variation in acoustic parameters of bone and the presence of soft tissues. The goal of present study was to get insight in the sensitivity of acoustic wave propagation and of the identification of OCDs to variation in the acoustic parameters of bone and to the presence of soft tissues. First, analogous to previous studies performed by White et al. (2010) and Sarkalkan et al. (2014) a two dimensional finite-difference time-domain model of the ankle joint space was generated. Second, a sensitivity analysis was performed to analyse the influence of variation in the values of the acoustic parameters (such as the density, Lamé's constants and bulk and shear viscosity) of bone. Third, the acoustic parameters of Achilles tendon and skin were determined experimentally. The experimentally determined acoustic parameters were used to add the soft tissue layers to the model of the ankle joint space to indicate their influence on acoustic wave propagation and on the identification of OCDs.

Materials & Methods

Throughout this study, two dimensional models of the ankle joint space were generated that included bone, the Achilles tendon and skin and two sets of computational simulations of acoustic wave propagation were performed by means of these models. Nerves, muscle and fat present in the ankle joint space were expected not to influence the acoustic wave propagation significantly. These soft tissues were therefore not taken into account. The density (ρ), Lamé's constants (λ & μ) and bulk (β) and shear (η) viscosity were the acoustic parameters required for the computational model. To assess the influence of the acoustic parameters on acoustic wave propagation simulations were performed

using mean, minimal and maximal values for the acoustic parameters of bone. The effect of the presence of soft tissues were assessed by gradually adding the tissue layers of skin and Achilles tendon to the ankle joint space models.

Two dimensional simulation model of the ankle model

To perform the simulations a geometry of the object of interest had to be built in the software package and starting conditions had to be defined**.** In our previous study simulations were performed on a simplified model of the ankle joint space (10). We adapted this model on the following points: 1. a more realistic geometry of the ankle joint space was created, and 2. layers of Achilles tendon and skin were added gradually to the model. One OCD location and OCD size were used during the entire study (Figure 1).

A model was created that represents the tibia and talus bone, which forms the basis of the ankle joint space. This model was given two conditions: first, the tibia and talus were intact forming the ankle joint space of a healthy ankle joint space and second, the talus was given an OCD with size of 5 mm wide and 5 mm deep in the middle of the talar role (Figure 1). An OCD of 5 mm wide and 5 mm deep can be classified as a small OCD which is of primary interest of the proposed diagnostic technique, but it was expected to be big enough for the identification of deviations in the output signals(13). The geometry of the tibia and talus are based on a CT scan that matched best with a mean shape of a statistical shape model built of the tibia and talus bone based on a database of 72 CT scans of human ankles. The CT images were segmented in Mimics® (Materialise, Leuven, Belgium). The CT-slices on which the talus could be seen ranged from 54.6 until 103.5. Slice 79.05 was taken to create the geometry for the model because it was assumed that this slice showed the ankle joint space in the middle of the ankle. In Figure 1, the synovial fluid is represented by the black colour, whereas the tibia and the talus bone are represented by the grey colour. The width of the ankle joint space was 2.5 mm which was based on the ankle joint space width of the CT scan that was used to create the model.

To assess the influence of the presence of the soft tissue Achilles tendon and skin were added gradually to the model (Figure 1). The thickness of Achilles tendon and skin were determined experimentally (Table 1).

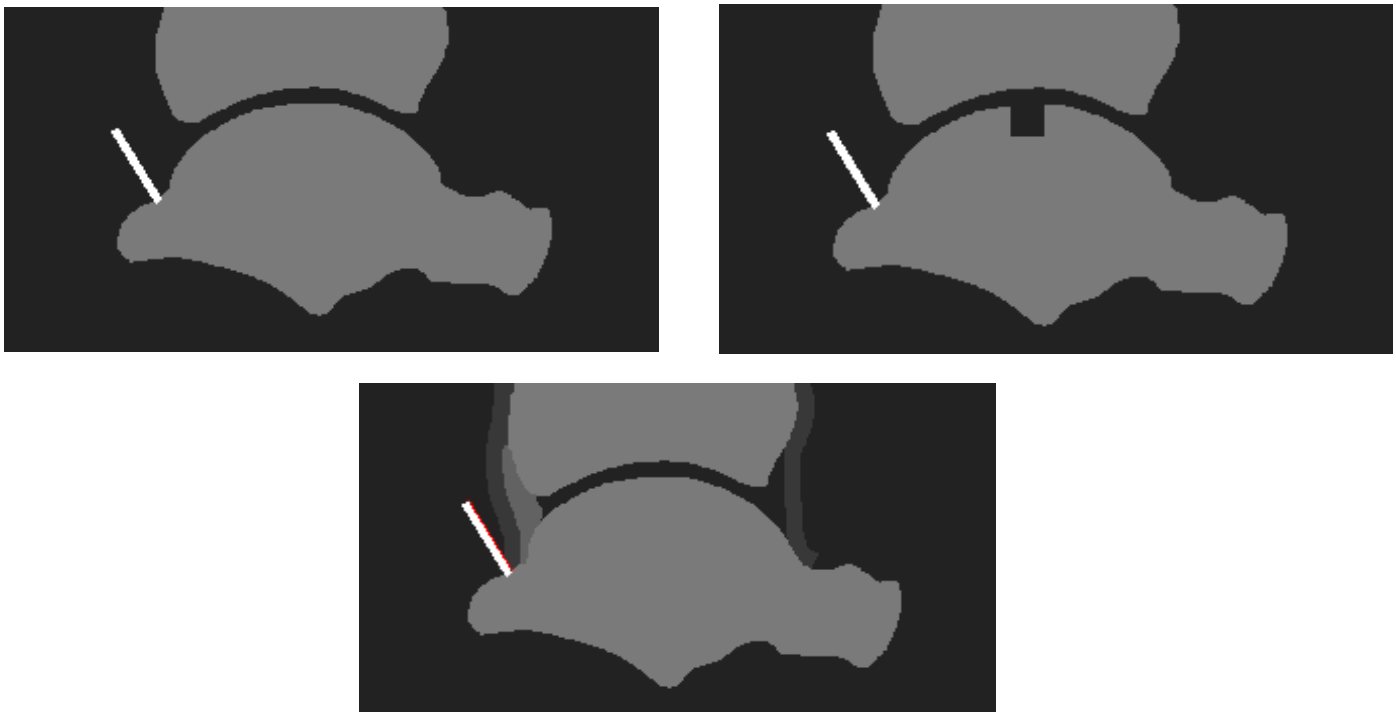

Figure 1: The conditions of the model that was created of the ankle joint space: top left: healthy ankle joint space, top right: ankle joint space with an OCD of 5 mm wide and 5 mm deep, bottom: ankle joint space with Achilles tendon and skin.

Based on our previous study it was assumed that the placement of a transmitter perpendicular to the opening of the ankle joint space results in acoustic wave propagation through the ankle joint space (11). Therefore, a non-focused transmitter (diameter: 12.7 mm) of 1 MHz was placed outside the ankle joint space with an angle of 60° (Figure 2). The distance between the transmitter and the ankle joint space should be as close as possible because this distance influences the intensity of the acoustic waves. A distance of 10 mm was used to ensure that there was enough space to add the layers of Achilles tendon and skin. One receiver was placed on the outside of the ankle joint space in an angle of 60°. One receiver was placed inside the ankle joint space close to the posterior opening of the joint, one in the middle of the ankle joint space, and one close to the anterior opening of the ankle joint space (Figure 2). The default settings for the receiver were: gain (0 dB), blanking (0 µs) and duration (0 µs).
Infinite boundary conditions were assigned to the four sides of the model. Infinite boundary conditions result in an encircled simulation volume (i.e. an infinite volume)(14). A grid size of (50µm) was used. Total simulation time was 100 µs.

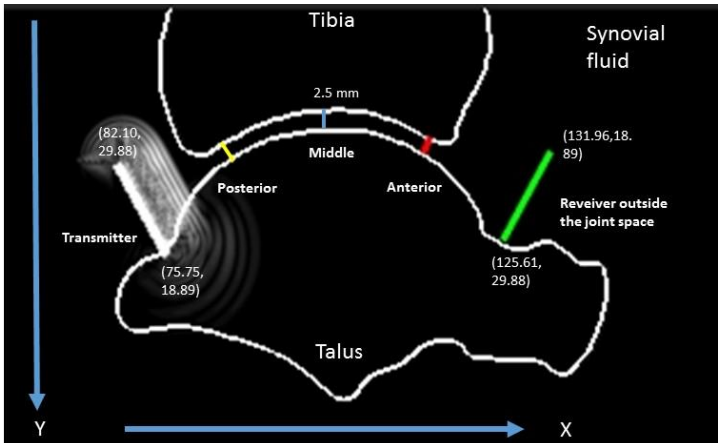

Figure 2: Model of the ankle joint space with the transmitter and four receivers that were placed to assess acoustic wave propagation through the joint space.

All simulations were performed using the software package Wave2000 (Cyberlogic Inc., New York, NY, USA). This software package uses the equation for acoustic wave propagation as presented in Equation 1 based on the algorithm described by Schechter et al.(1994)(15). This equation is based on the assumption that a heterogeneous material consists of homogeneous linear isotropic regions and that this material imposes continuity of stresses and displacements across boundaries of four homogenous regions. The surface of the model was divided in grid points. Within each grid element Equation 1 was solved. The displacement vector was computed at the intersection of four grid elements for each iterated time step during the simulations (Figure 3).

$$\rho \frac{\partial^2}{\partial t^2} = \left|\mu + \eta \frac{\partial}{\partial t}\right| \nabla^2 w + \left|\lambda + \mu + \beta \frac{\partial}{\partial t} + \frac{\eta}{3}\frac{\partial}{\partial t}\right| \nabla (\nabla * w) \qquad \text{(Equation 1)}$$

where w is a 2D vector whose components are the x and y components of displacement of the material at a location (x, y), ρ is the material density (kg/m^3), λ is the first Lamé's constant (Pa), µ is the second Lamé's constant (Pa), η is the shear viscosity (Pa ·s), β is the bulk viscosity (Pa ·s), t is the time (s), ∂ is

the partial difference operator, ∇^2 is the Laplace operator, and ∇ is the divergence operator.

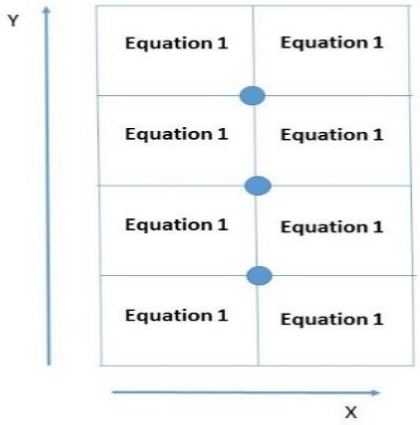

Figure 3 : The surface of the model was divided in grid points. Equation 1 is computed for each grid point, the displacement vector (w(x), w(y)) was computed at the intersection of four grid elements for each iterated time step (indicated by the dots).

Propagating acoustic waves encounter particles within the medium. Different phenomena occur which influence acoustic wave propagation: 1. when acoustic waves meet a boundary between tissues with different acoustic parameters, part of the waves are reflected whereas another part is transmitted. This decreases the amplitude of the acoustic waves. 2 Acoustic wave propagation is influenced by the acoustic parameters that are described in Equation 1 in a relation described by Equation 2. The propagating speed decreases with increasing density, while the propagating speed increases with increasing stiffness (I.e. resistance of the material to deformation by an applied force). The stiffness of the medium is described by the Lamé's constants in Equation 1. 3. The damping parameters (shear and bulk viscosity) influence the amplitude of the propagating waves because they represent the amount of scattering and absorption that occurs during acoustic wave propagation, which leads to a decrease in amplitude with increased damping(16).

$$C = \sqrt{\frac{K}{\rho}} \text{ (16)} \qquad \text{(Equation 2)}$$

where C is the propagating speed(m/s) of the acoustic waves, K represents the stiffness of the medium (Pa)(described by the Lamé's constants within Equation 1), and ρ is the density (kg/m^3) of the medium.

Acoustic parameters

Acoustic parameters required for the computational model

The first and second Lamé's constants were calculated by the density, and the longitudinal (V_l) and shear (V_t) acoustic velocity (Equation 3 and Equation 4). Longitudinal waves cause a displacement of particles in the medium that is parallel to the direction of the waves motion. For transverse waves, the displacement of particles is perpendicular to the direction of propagation(16). The shear velocity of Achilles tendon and skin were not described in literature and we calculated them by the longitudinal velocity and the Poisson's ratio (ν) (Equation 5). The Poisson's ratio(ν) of materials with a small modulus of rigidity are close to 0.5, which means that the materials are nearly incompressible (the materials volume is conserved after deformation).Therefore, a Poisson's ratio of 0,4999 was used to ensure that the calculated values for the shear velocity of Achilles tendon and skin were realistic and that the soft tissues were nearly incompressible(12).

First Lamé's constant (16-18):

$$\lambda = \rho\left(V_l^2 - 2\,V_t^2\right) \quad \text{(Equation 3)}$$

Second Lamé's constant (16, 18):

$$\mu = \rho(V_t^2) \quad \text{(Equation 4)}$$

Shear velocity (17):

$$\mathrm{V_t} = \sqrt{\frac{1-2\nu}{(1-\nu)^2}}\,V_l \quad \text{(Equation 5)}$$

The shear and bulk viscosity values depend on the attenuation (α), the computational model distracts the shear and bulk viscosity automatically. The shear and bulk viscosity were calculated by the simulation software based on the attenuation that was described by literature for bone, and based on the experimentally determined attenuation for Achilles tendon and skin (Table 1). No information was provided about the formula used by the simulation software. Literature describes the relation between the attenuation, the shear and bulk viscosity by Equation 6). It was therefore assumed that the computational software distracts the shear and bulk viscosity based on this relation.

Attenuation (17, 19, 20):

$$\alpha = \frac{4\pi^2 f^2(\eta + 3\frac{\beta}{4})}{\rho V} \quad \text{(Equation 6)}$$

Where f is the frequency (MHz),ρ is the density (kg/m^3) and V = acoustic velocity (m/s), η is the shear viscosity and β is the bulk viscosity.

Acoustic parameters used for the sensitivity analysis

The effect of variation in acoustic parameters of bone and the presence of soft tissues were assessed by a sensitivity analysis. Acoustic parameters were assigned to each tissue present in the model of the ankle joint space. The acoustic parameters of bone are described sufficiently in literature (Table 1). The acoustic parameters of skin and Achilles tendon were determined experimentally (Table 1). The acoustic parameters of synovial fluid were not described in literature but the values for water described by the material library of the computational model were used following our previous study and the study performed by White et al (2010)(10, 21) (Table 1). It was assumed that the viscosity of synovial fluid is lower than that of water. Hence, a shear viscosity of 0.01 Pa ·s was used instead of 0.001 Pa ·s (22).

Experiment: Acoustic parameters of skin and Achilles tendon

Specimen

For the experiments tissues from frozen human cadaver ankles were used. The cadaver ankles were defrosted and dissected. The tissue samples were frozen again after dissection and defrosted again a few hours before the experiments. No information about the age or freshness was available.

For the determination of the thickness (l), longitudinal velocity and attenuation 6 different cadavers were used. The tissues were collected and cut in to pieces of 5 cm x 5 cm. This resulted in 8 samples of Achilles tendons and 3 skin samples.
For the determination of the density 6 other cadaver ankles were used. The following samples were collected: 6 Achilles tendons and 3 skin samples.

Pulse echo method and density bottle method

The thickness, longitudinal velocity and attenuation of skin and Achilles tendon were determined by the use of the Macro scanner (TU Delft, The Netherlands) that is based on the pulse-echo method(23). The measurements with samples that were placed on top of the reflector plate were compared with a reference measurement without samples, similar as described by Parker et al. (1983)(24)(Figure 4). One spherically focused transducer with centre frequency 5 MHz and focal distance 38 mm (Olympus, United states of America) was used that both acted as source and receiver. The pulses were generated by a square wave pulser and receiver unit (Panametrics-NDT 5077PR Olympus, Massachusetts, United States of America). Pulses were emitted with a pulse repetition frequency of 2 kHz and a pulser voltage of 100 V. A high pass filter of 1 MHz and a low pass filter of 10 MHz were used to filter the output. The transmitted waves were sent through the sample and reflected by a reflector plate aligned perpendicular to the transducer. The signals were read out by an oscilloscope with a sampling rate of 50 MHz (Agilent DSO7054A, KeySight technologies, Amsterdam, The Netherlands). Four samples were placed next to each other on the reflector plate and their entire surface was scanned once with a grid size of 2mm. This resulted in a large number of grid points per sample (approx. 400 grid points per skin sample, and 600 for each Achilles tendon sample). The values of the acoustic parameters were averaged over all grid points per sample. A total average value and standard deviation per tissue were computed with the mean values of each individual sample per tissue. The frequency dependent attenuation was determined. We used the attenuation at 1 MHz throughout the present study. Phosphate buffered saline (PBS) was used as background medium to mimic in vivo conditions. The measurements were performed at 37℃.

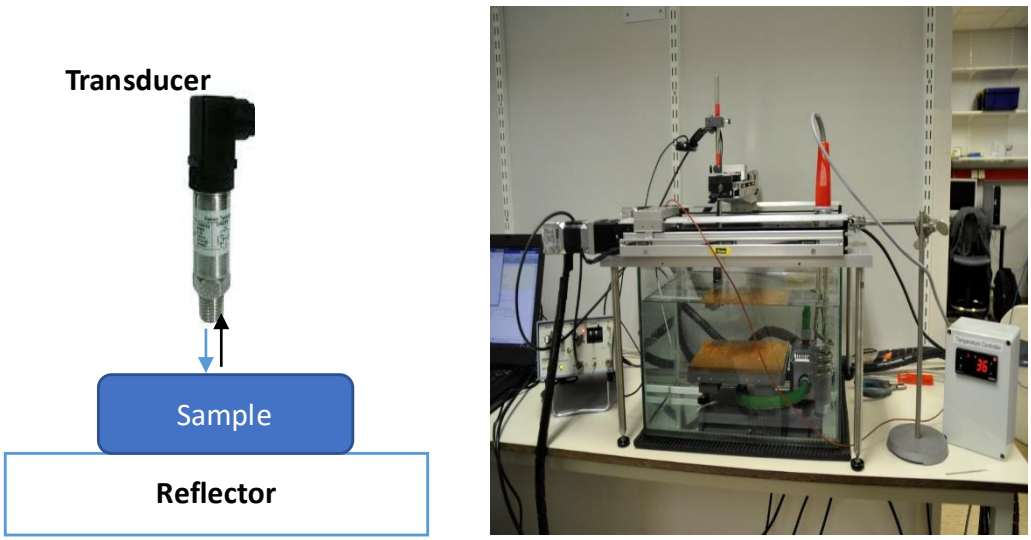

Figure 4: A transducer that acted as source (transmitted acoustic waves, blue arrow) and receiver (collected acoustic waves, black arrow) was placed above the samples that were placed on top of the reflector plate. Right: the whole set-up, that consist of a water tank (with PBS), the transducer and reflector plate, a heating system and a motor system that was used to scan the entire surface of the samples.

The density of skin and Achilles tendon were determined by the use of the density bottle method as described by DiResta et al.(1990) (25).Two pycnometers (2,17 mL, Fisher Inc, Ottowa, Canada) were used. Each sample was cut into pieces and two measurements per sample were performed. For each individual sample the mean value of the two measurement was computed. A total average value and standard deviation per tissue were computed with the mean values of each individual sample per tissue. Phosphate buffered saline (PBS) was used as background medium to mimic in vivo conditions. Measurements were performed at 37℃. The data processing steps that were executed to determine the thickness, longitudinal velocity, attenuation and density are extensively described in Appendix C.

Data analysis

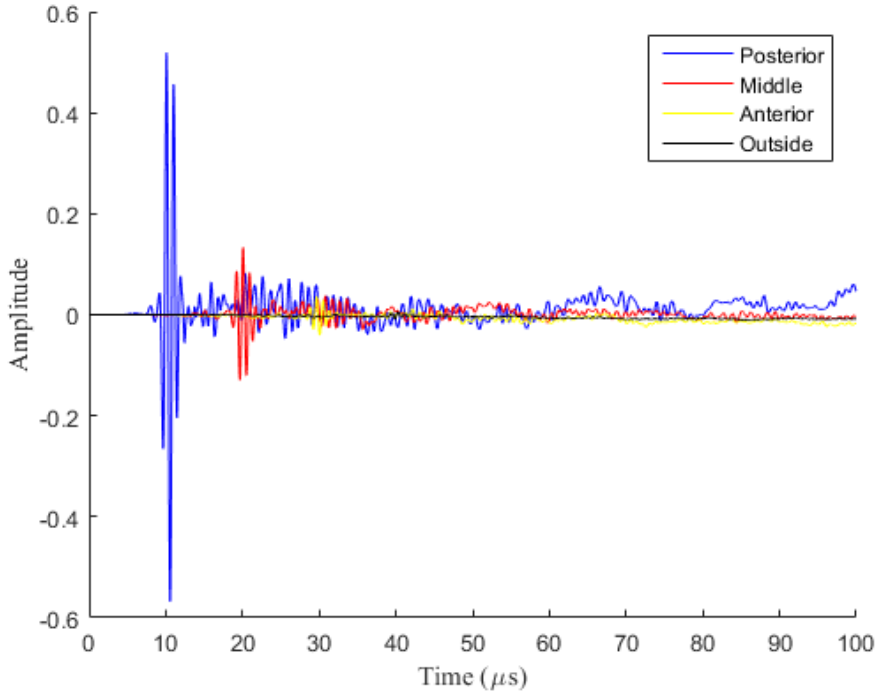

Figure 5: The output signals of the receivers that were placed posterior, middle and anterior in the joint space and the transmitter that was placed outside the joint space.

Output signals

The amplitude of the propagating waves decreased with time (Figure 5). The amplitudes of the waves that were collected by the receiver inside the ankle joint space close to the posterior opening are in the range of 0.6. The receiver in the middle of the ankle joint space collected waves with amplitudes in the range of 0.15. The receiver inside at the anterior opening of the ankle joint space collected waves with amplitudes in the range of 0.04. The receiver outside the ankle joint space collected waves with a small amplitude in the range of $1 \cdot 10^{-3}$ (Figure 6). The output signal of the receiver that was placed outside the ankle joint space was of main interest for the present study because this is the signal that will be assessed in the clinic when the proposed diagnostic technique will be used. The output signals of the receiver in the middle of the ankle joint space and on the anterior side of the ankle joint space were assessed in present study to get more insight in the behaviour of the waves within the ankle joint space.

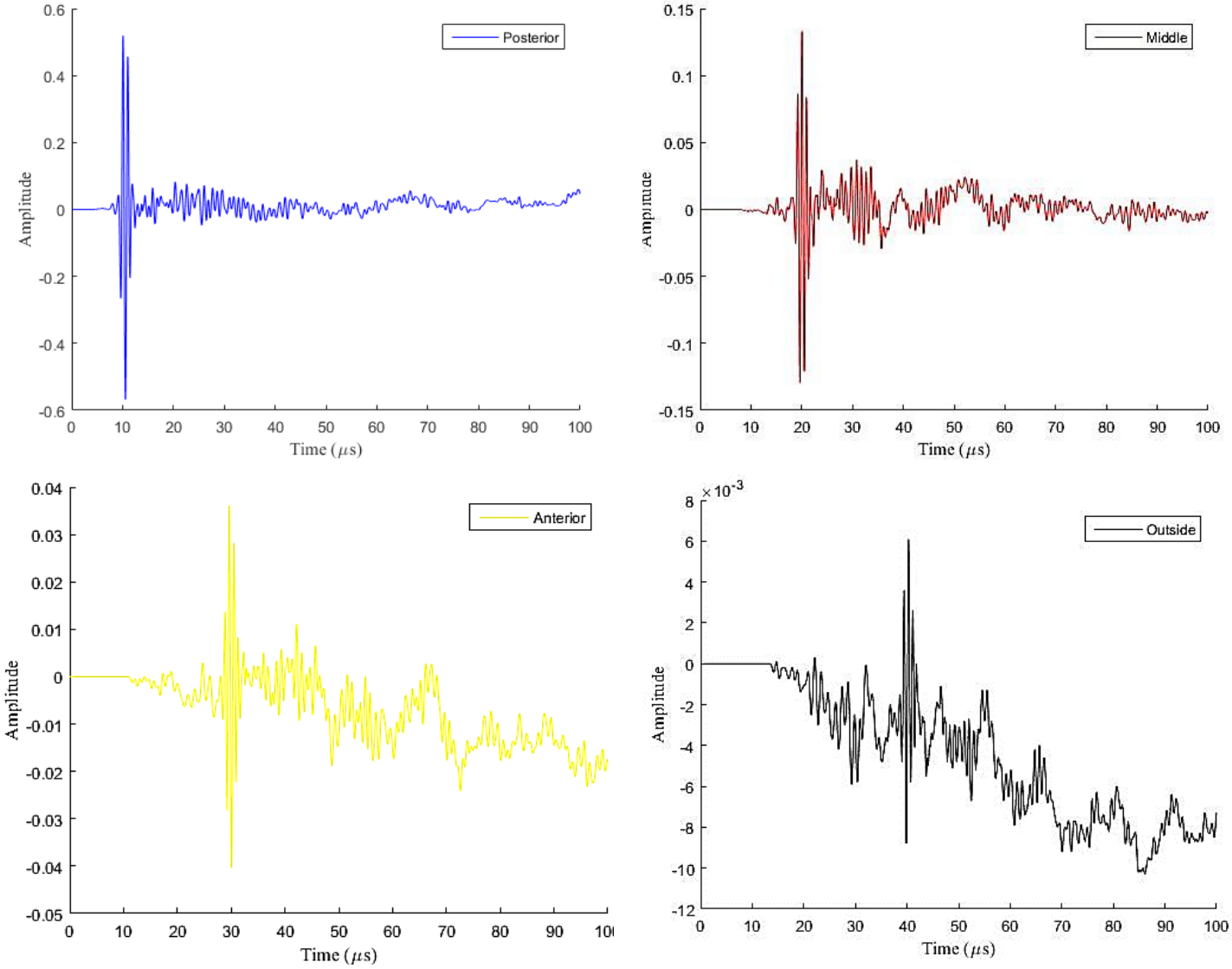

Figure 6 : The output signals of the receiver in the posterior, middle, anterior side and outside of the joint space.

Assessment of the sensitivity of acoustic wave propagation

The normalized root mean square error (NRMSE) and the normalized maximum cross correlation (NMCC) were used to assess the sensitivity of acoustic wave propagation analogous to our previous study(10).For the data processing, the software package Matlab R2015b (The MathWorks, Inc., Natick, Massachusetts, United States of America) was used.

The first sensitivity assessed was the sensitivity for variation in the acoustic parameters of bone. We refer to this as the min/max sensitivity. We studied this by modelling wave propagation for the minimal and maximal values of acoustic parameters found in literature. The minimal and maximal values of the acoustic parameters of bone described in literature were used for the sensitivity analysis because it was assumed that they represent the natural range of possible values in acoustic parameters. The mean relative difference (100 *|mean – minimal or maximal value|/mean) from the mean for minimal and maximal acoustic parameter values for bone was largest (50%) for the first

Lamé's constant and the shear viscosity, 30% for the second Lamé's constant and 30 % for the bulk viscosity. The density had the smallest mean relative difference (15%). The five acoustic parameters were divided into three sets of acoustic parameters. 1. Density, 2.the first and second Lamé's constants and 3.the bulk and shear viscositiy. The Lamé's constants and the bulk and shear viscosity were combined in one set because both acoustic parameters represent the stiffness (Lamé's constants) and amount of attenuation (viscosities). One set of acoustic parameters (density, Lamé's constants or the bulk & shear viscosity) were changed to its minimal or maximal value (altered situation) at a time, while the other acoustic parameters were kept at their mean values.

The second sensitivity studied was the sensitivity for presence of soft tissues. We did this by adding skin and Achilles tendon gradually (first Achilles tendon, then skin) and assessing the wave propagation (altered situation). The mean values of the experimentally determined acoustic parameters were used for the calculation of the acoustic parameters of Achilles tendon and skin required for the simulation model. We refer to this as the soft tissue sensitivity. Min/max sensitivity and soft tissue sensitivity were estimated by comparing wave propagation in the altered situation with a reference situation with mean values for acoustic parameters of bone.

The third sensitivity studied was the one for an OCD. This was done by studying the differences in wave propagation between healthy (reference situation) and defected ankles (altered situation) under similar simulation conditions (Figure 7). We refer to this sensitivity as the defect sensitivity. The sensitivities were assessed for the receivers that were placed in the middle, anterior and outside of the ankle joint space.

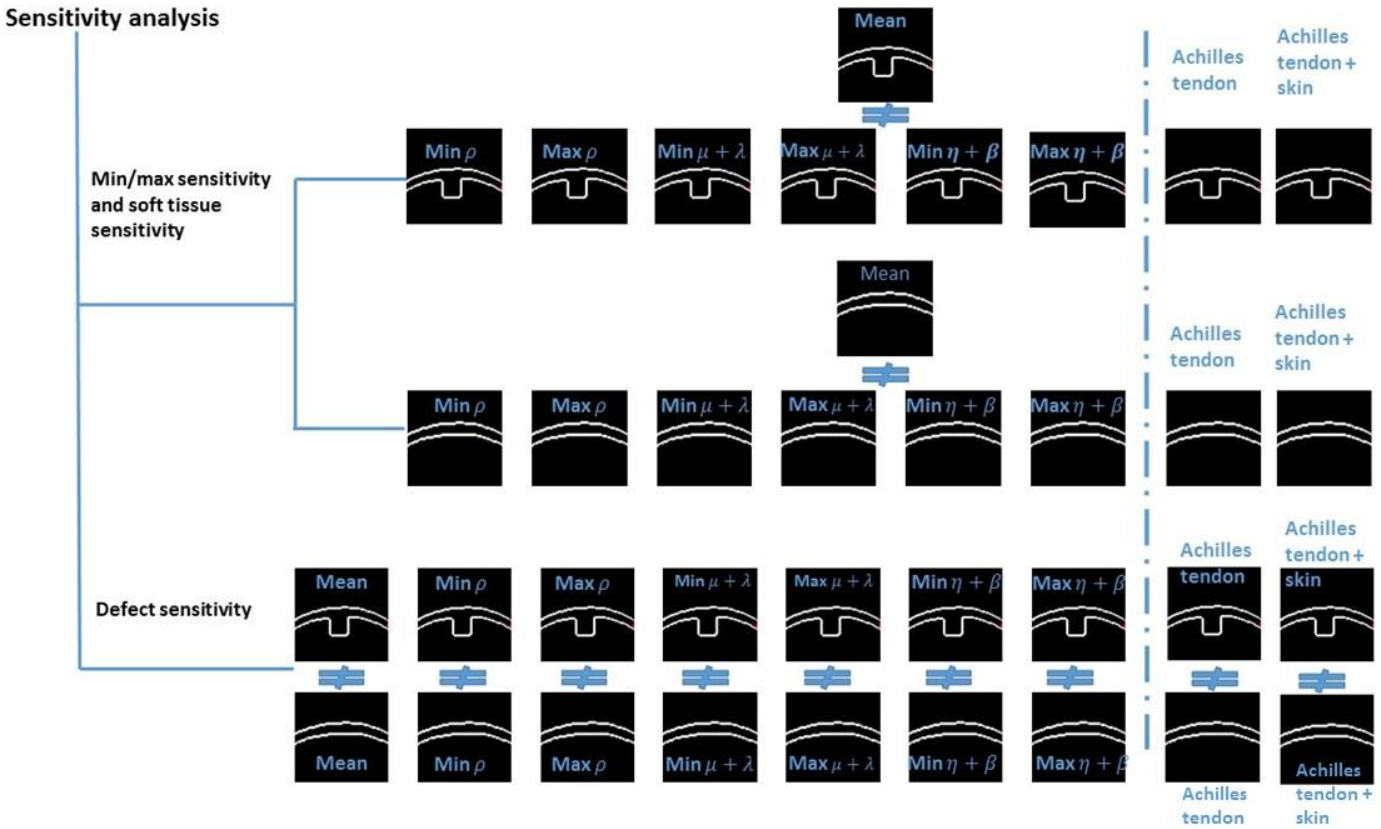

Figure 7: Flowchart of the min/max, soft tissue and defect sensitivity.

NRMSE

The NRMSE was calculated to determine the difference between the output signals of the altered situation and reference situation. We assumed that an NRMSE under 1 % resembles two signals that are similar based on our previous study. The higher the NRMSE the larger the difference between the output signals of the altered and reference situation.

$$NRMSE = \frac{\sqrt{\frac{\sum_{i=1}^{n}\left(x_{obs,i}-x_{ref,i}\right)^2}{n}}}{x_{obs,max}-x_{obs,min}}\ x\ 100\ \% \qquad (6)$$

where $x_{obs,i}$ is the amplitude of the altered signal at time i, $x_{ref,i}$ = amplitude of reference signal at time i, $x_{obs,max}$ = maximum amplitude of the altered signal, $x_{obs,min}$ = minimum of the altered signal, n = the number of amplitude values obtained for each simulation condition(10).

NMCC

The NMCC was calculated because it is invariant to time shift. The shape of the signal is therefore represented in more detail by the NMCC than the NRMSE. The NMCC was used to indicate whether the various simulation conditions influence the shape of the signal.

$$NMCC = \frac{\max|(f*g[i])|}{\sqrt{\sum_{i=1}^{n} f[i]^2}\sqrt{\sum_{i=1}^{n} g[i]^2}} \qquad (7)$$

f and g are two output signals, n = the number amplitude values obtained of each signal, $(f * g[i])$ is the cross correlation of the two output signals. When the NMCC is higher than 0.95 than is the shape of the signal of the altered situation similar to the reference situation.(10).

Maximum absolute amplitude of the signal

The amplitudes of the output signals were influenced by variation in acoustic parameters of bone and the presence of soft tissues (Figure 8). To compare these effect on the amplitudes, the maximum amplitude of each output signal was determined. First, the part of the output signal where the amplitudes abruptly changed into larger values and where it abruptly changed into lower values was selected automatically by the software as the area which contains the largest peaks of each output signal. The largest peaks of the output signal occurred around the same time for each receiver. It was therefore checked if the selected area with the largest peaks of the signal were in the expected time frame. Within the selected area, the difference between the minimum and maximum value of the amplitude was determined to calculate the absolute maximum amplitude of each output signal.

Time shift

The variation in the acoustic parameters of bone and the presence of soft tissues influences the propagation speed of the acoustic waves. The propagation speed affects the moment in time at which the waves are collected by the receivers. The time at which the receivers started to collect the acoustic waves of the altered simulations were compared to the reference situations (Figure 8). The time shift was calculated by comparing these points in time. This resulted in a negative time shift when the acoustic waves were received earlier than the acoustic waves of the simulations with the mean acoustic parameters of bone, positive when the opposite occurred.

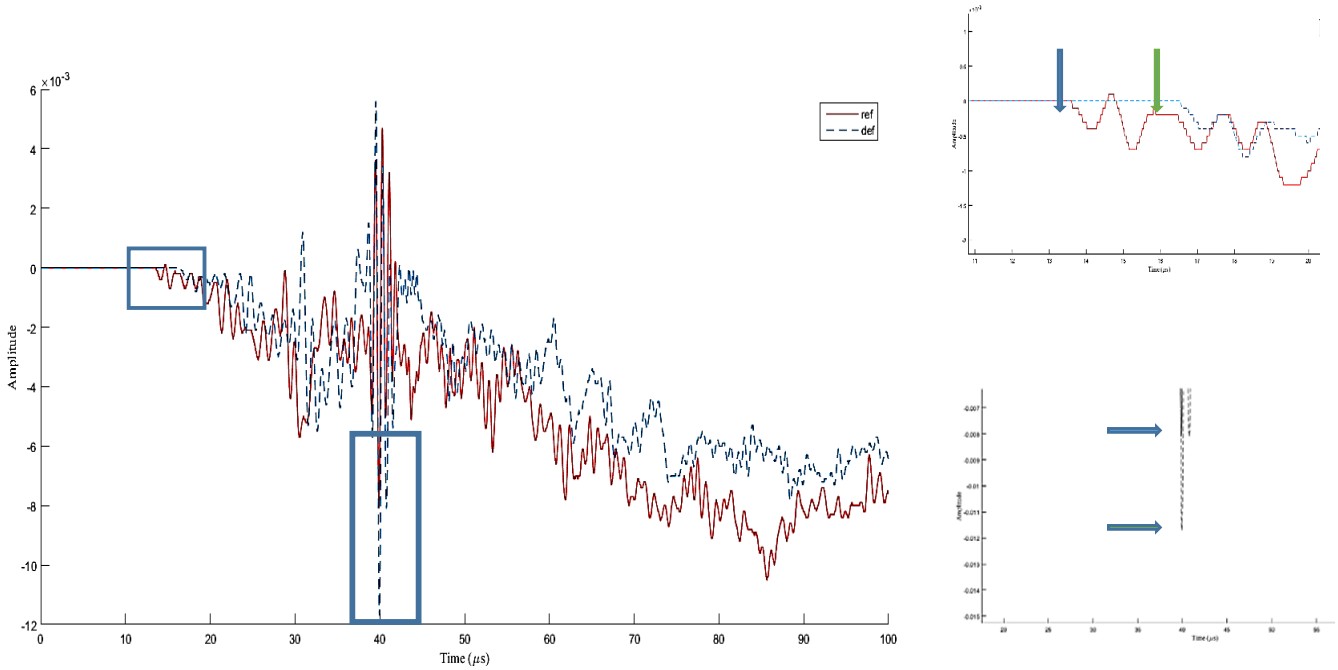

Figure 8: Output signal between the reference mean ankle (red) with an ankle with maximal density of bone (blue stripes), the time shift and change in amplitude are indicated in the boxes in the graph left. The time shift is indicated in the graph on the right (top) and the change in the amplitude in the right (bottom).

Results

Table 1 presents the acoustic parameters that were acquired from literature for bone, from the material library of the computational software for synovial fluid, and from our experiments for skin and Achilles tendon and those that were subsequently calculated for the computational simulations. The experimentally determined thickness, density and longitudinal velocity of skin and Achilles tendon showed less variation compared to the experimentally determined attenuation.

Table 1 : Overview of the acoustic parameters of bone, synovial fluid, skin and Achilles tendon. Abbreviations: V_l = longitudinal velocity, V_t = shear velocity, α = attenuation, l = thickness, ρ = density, λ = first Lamé's constant, μ = second Lamé's constant, η = shear viscosity, β = bulk viscosity. * Experimentally determined values expressed as mean (standard deviation), # Values described by literature expressed as mean (standard deviation) ǂ values provided in the material library of the computational model, ¥values calculated by use of the Poisson ratio (0.4999) (Equation 5), + mean (min-max) values found in literature. Values were calculated with; a = Equation 3, b= Equation 4, c = Equation 6. For skin and Achilles tendon the mean experimentally determined values were used for the calculation of the acoustic parameters required for the computational model.

Tissue	V_l (m/s)	V_t (m/s)	α (dB /cm/MHz)	l (mm)	ρ (kg/m^3)	λ^a (MPa)	μ^b (MPa)	η^c (Pa ·s)	β^c (Pa·s)
Cortical bone	*3177 (470)[26-28]#*	*1478(137)[29]#*	12(9)[14, 27]#	-	1705(1550 – 1970) +	9770(6069 – 14669) +	3719(2708 – 4923) +	40 (20 -60) +	0.1 (0.07 – 0.13) +
Synovial fluid	-	-	-	-	1000ǂ	2241ǂ	0	0.01ǂ	$9.9 \cdot 10^{-8}$ ǂ
Skin	1187 (29) *	106¥	0.86 (0.4) *	2.5 (0.95) *	1517 (1) *	3424	16	0.88	$7.9 \cdot 10^{-8}$
Achilles tendon	1574 (14) *	140¥	1.2 (1.5) *	4.6 (1.7) *	1512 (70) *	3684	29	0.32	$2.0 \cdot 10^{-4}$

Receiver outside the ankle joint space

Table 2 presents the NRMSE, NMCC, maximum absolute amplitude and time shift of the output signals of the simulations collected by the receiver outside the ankle joint space.

Min/max sensitivity

The NRMSE for the condition with OCD was lower than for the healthy condition. The NRMSE was smallest for the minimal bulk and shear viscosity in the healthy condition. The NMCC values were close to 0.95 for both ankle conditions. The time shift caused by the density and Lamé's constants was the same for both ankle conditions. No time shift caused by the bulk and shear viscosity was found. The smallest amplitude was found for the maximal density and the largest amplitude for the maximal Lamé's constants for both ankle conditions.

Defect sensitivity

The NRMSE was larger than 1 % for both the min/max and the defect sensitivities. The NRMSE for the defect sensitivities were lower than for the min/max sensitivities (Figure 9). The NMCC values were above 0.95 which is in the same range as for the min/max sensitivities.

Receiver in the middle of the ankle joint space

Table 3 presents the NRMSE, NMCC, maximum absolute amplitude and time shift of the output signals bone collected by the receiver in the middle of the ankle joint space.

Min/max sensitivity

The NRMSE was the smallest for minimal and maximal bulk and shear viscosity in the healthy condition and the maximal bulk and shear viscosity in the condition with an OCD. The NRMSE for the healthy condition were lower than for the defected condition. The NMCC was close to 0.70 for the density and Lamé's constants for both ankle conditions, the NMCC for the bulk and shear viscosity was high for both ankle conditions (close or above 0.95). The time shift caused by the density and Lamé's constants was different between both ankle conditions, and no time shift was found for the bulk and shear viscosity. The smallest amplitude was found for the maximal density in the healthy condition, and for the maximal density and minimal Lamé's constants in the defected condition. The largest amplitude was found for the minimal density in both ankle conditions.

Defect sensitivity

The NRMSE was larger than 1 % for both the min/max and the defect sensitivities. The NRMSE values of the defect sensitivities were higher than of the min/max sensitivities (Figure 9). The NMCC of the defect sensitivities was around 0.55 this was lower than the NMCC for the min/max sensitivities of both ankle conditions.

Receiver at the anterior side of the ankle joint space

Table 4 presents the NRMSE, NMCC, maximum absolute amplitude and time shift of the output signals collected by the receiver at the anterior end of the ankle joint space.

Min/max sensitivity

The NRMSE for the bulk and shear viscosity were low compared to the density and Lame's constants for the healthy condition. A low NRMSE for the maximal bulk and shear viscosity was found for the condition with an OCD. The NRMSE for the condition with OCD was lower than for the healthy condition. The NMCC was close to 0.80 for the density and Lamé's constants for both ankle conditions, whereas the NMCC for the bulk and shear viscosity were higher than 0.95 for both ankle conditions. The time shift caused by the density and Lamé's constants was different between both ankle conditions, and no time shift was found for the bulk and shear viscosity. The smallest amplitude was found for the minimal Lamé's constants in the healthy condition, and for the mean, maximal density

and maximal bulk and shear viscosity in the defected condition. The largest amplitude was found for the density in the healthy condition, and for the Lamé's constants in the defected condition.

Defect sensitivity

The NRMSE was larger than 1 % for both the min/max and the defect sensitivities. The NRMSE of the defect sensitivities were smaller than of the min/max sensitivities. NMCC values of the defect sensitivities were around 0.95. This is higher than the NMCC of around 0.80 of the min/max sensitivities for density and the Lamé's constants.

Soft tissue sensitivity

Table 5 presents the NRMSE, NMCC, maximum absolute amplitude and time shift of the output signals of the simulations with the presence of Achilles tendon or Achilles tendon and skin collected by the three receivers.

The NRMSE was larger than 1 % for both the soft tissues and the defect sensitivities. The soft tissue sensitivities based on the NRMSE were in the same range as the min/max sensitivity for the three receivers. The NRMSE for the addition of skin was higher than for the addition of Achilles for all three receivers. The largest effect on the NRMSE caused by the addition of Achilles tendon and skin was found for the receiver outside the ankle joint space for both ankle conditions. The NMCC was larger when only Achilles tendon was added compared to the NMCC of Achilles tendon and skin. No time shift was found. The amplitudes of the situations with Achilles tendon and skin were lower than the amplitude of the reference situation.

Defect sensitivity

The NRMSE for the defect sensitivities for bone with Achilles tendon and skin were higher than for bone alone for all three receivers. For the receivers at the anterior and at the outside of the ankle joint space the defect sensitivities were smaller than the soft tissue sensitivities. The defect sensitivities were larger than the soft tissue sensitivities for the receiver in the middle of the ankle joint space. And a noticeable difference in NMCC for the defect sensitivities compared to the soft tissue sensitivities were found for the receiver in the middle of the ankle joint space which was not present for the receivers at the anterior and at the outside of the ankle joint space.

Figure 9 gives a graphical representation of the NRMSE for the min/max and defect sensitivities for both ankle conditions for the receiver outside and in the middle of the ankle joint space. For the receiver outside the joint space the defect sensitivities were lower than the min/max sensitivities for both ankle conditions. Whereas the min/max sensitivities were lower than the defect sensitivities for the receiver that was placed in the middle of the joint space. For both receivers the range of the defect sensitivity for each acoustic parameter is smaller than for the min/max sensitivities. Since the relation between the min/max and defect sensitivities is similar in the receiver on the anterior and outside of the joint space only the NRMSE values for the receiver on the outside of the joint space were displayed.

Table 2: Receiver outside the ankle joint space: NRMSE, NMCC, maximum absolute amplitude and time shift for the min/max and defect sensitivities of both ankle conditions.

		ρ (kg/m^3)		**λ** & **μ** (MPa)		**η** & **β** (Pa·s)	
Healthy ankle: min/max sensitivity	Mean	Min	Max	Min	Max	Min	Max
NRMSE (%)	-	11	16	13	8.0	6.0	8.0
NMCC	-	0.94	0.95	0.94	0.95	0.99	0.99
Time shift (μs)	-	-1.2	1.1	2.9	-2.1	0.0	0.0
Amplitude	0.014	0.016	0.010	0.015	0.019	0.018	0.014
Ankle with OCD: min/max sensitivity							
NRMSE (%)	-	10	11	11	8.0	10	8.0
NMCC	-	0.95	0.97	0.96	0.97	0.99	0.98
Time shift (μs)	-	-1.2	1.1	2.9	-2.1	0.0	0.0
Amplitude	0.012	0.014	0.011	0.017	0.018	0.016	0.013
Defect sensitivity							
NRMSE (%)	5.0	5.0	7.0	6.0	5.0	8.0	5.0
NMCC	0.99	0.95	0.96	0.95	0.96	0.98	0.98

Table 3:Receiver in the middle of the ankle joint space: NRMSE, NMCC, maximum absolute amplitude and time shift for the min/max and defect sensitivities for both ankle conditions.

		ρ (kg /m^3)		**λ** & **μ** (MPa)		**η** & **β** (Pa·s)	
Healthy ankle: min/max sensitivity	Mean	Min	Max	Min	Max	Min	Max
NRMSE (%)	-	7.0	8.0	8.0	8.0	3.0	1.0
NMCC	-	0.70	0.74	0.78	0.60	0.96	0.99
Time shift (μs)	-	-0.68	0.61	1.6	-1.8	0.0	0.0

Amplitude	0.26	0.32	0.23	0.31	0.30	0.28	0.24
Ankle with OCD:							
Min/max sensitivity							
NRMSE (%)	-	8.0	10	10	9.0	8.0	1.0
NMCC	-	0.64	0.78	0.70	0.65	0.92	0.99
Time shift (µs)	-	-0.49	1.4	1.5	-1.0	0.0	0.0
Amplitude	0.11	0.14	0.10	0.10	0.11	0.13	0.11
Defect sensitivity							
NRMSE (%)	11	10	11	11	12	11	12
NMCC	0.52	0.60	0.53	0.55	0.53	0.35	0.55

Table 4:Receiver on the anterior side of the ankle joint space: NRMSE, NMCC, maximum absolute amplitude and time shift for the min/max and defect sensitivities for both ankle conditions.

		$\boldsymbol{\rho}$ (kg/m^3)		$\boldsymbol{\lambda}$ & $\boldsymbol{\mu}$ (MPa)		$\boldsymbol{\eta}^{\&}\boldsymbol{\beta}$ (Pa·s)	
Healthy ankle: min/max sensitivity	Mean	Min	Max	Min	Max	Min	Max
NRMSE (%)	-	10	10	13	7.0	5.0	2.0
NMCC	-	0.81	0.78	0.82	0.83	0.98	0.99
Time shift (µs)	-	-0.95	0.90	2.4	-1.7	0.0	0.0
Amplitude	0.070	0.082	0.083	0.050	0.070	0.071	0.072
Ankle with OCD: min/max sensitivity							
NRMSE (%)	-	9.0	10	6.0	7.0	10	2.0
NMCC	-	0.81	0.85	0.83	0.81	0.94	0.99
Time shift (µs)	-	-0.84	0.86	2.1	-1,7	0.0	0.0
Amplitude	0.062	0.082	0.061	0.092	0.092	0.070	0.061

Defect sensitivity							
NRMSE (%)	4.0	4.0	4.0	3.0	4.0	3.0	4.0
NMCC	0.96	0.96	0.96	0.95	0.96	0.96	0.97

Table 5: NRMSE, NMCC, time shift and amplitude for the soft tissue and defect sensitivity for the three receivers.

	Receiver in the middle of the ankle joint space			Receiver on the anterior side of the ankle joint space			Receiver outside the ankle joint space		
	Mean	Bone + Achilles tendon	Bone +Skin & Achilles tendon	Mean	Bone + Achilles tendon	Bone +Skin & Achilles tendon	Mean	Bone + Achilles tendon	Bone +Skin & Achilles tendon
Healthy ankle: soft tissue sensitivity									
NRMSE (%)	-	4.0	5.0	-	6.0	14	-	9.0	53
NMCC	-	0.85	0.71	-	0.92	0.54	-	0.96	0.67
Time shift(µs)	-	0.0	0.0	-	0.0	0.0	-	0.0	0.0
Amplitude	0.26	0.22	0.22	0.081	0.062	0.062	0.014	0.011	0.011
Ankle with OCD: soft tissue sensitivity									
NRMSE (%)	-	9.0	10	-	9.0	14	-	7.0	66
NMCC	-	0.78	0.64	-	0.89	0.54	-	0.98	0,.5
Time shift(µs)	-	0.0	0.0	-	0.0	0.0	-	0.0	0.0
Amplitude	0.11	0.082	0.091	0.062	0.051	0.061	0.012	0.010	0.010
Defect sensitivity									
NRMSE (%)	11	15	13	4.0	6.0	6.0	5.0	7.0	10
NMCC	0,52	0,40	0,60	0,96	0,94	0,83	0.99	0.98	0,80

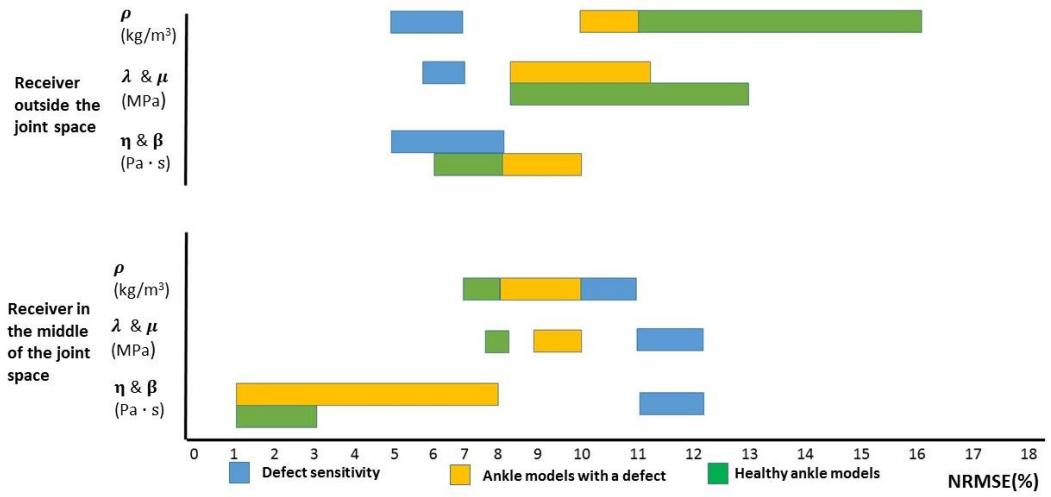

Figure 9 : Top: Min/max and defect sensitivities for both ankle conditions for the receiver outside the joint space. Bottom: Min/max and defect sensitivity for both ankle conditions for the receiver in the middle of the joint space.

Discussion

To study the potential of acoustic wave propagation to identify OCDs within the ankle joint space and the sensitivity of acoustic wave propagation to variation in acoustic parameters of bone and to the presence of soft tissue were the primary goals of present study.

A model that represents the tibia and talus bones, which form the basis of the ankle joint space, was created. This model was given two conditions: healthy and with an OCD with a size of 5 mm wide and 5 mm deep in the middle of the talar role. The output signals of receivers placed at the middle, the anterior and on the outside of the ankle joint space were assessed to gain information about the sensitivity of acoustic wave propagation. First the min/max sensitivity was studied, the minimal and maximal acoustic parameters of bone described by literature were changed step-by-step. The second sensitivity studied was the sensitivity for presence of soft tissues, by gradually adding layers of Achilles tendon and skin. The third sensitivity, the defect sensitivity was studied by comparing a healthy and a defected ankle with similar acoustic parameters.

Studies performed by Sarkalkan et al. (2014) and White et al. (2010) were based on simplified models of the ankle joint space that contained acoustic properties of Perspex(10, 11). It is expected that the geometries used in the present study based on a statistical shape model of the ankle joint space, and the acoustic parameters of bone, skin and Achilles tendon resemble the ankle joint space more accurately**.** The present study aimed to give insight in all aspects of the computational simulations. For further elaboration of the model used in our previous study acoustic parameters were assigned each tissue present in the simulation model. The acoustic parameters of bone were described by literature. The acoustic parameters of Achilles tendon and skin were determined experimentally as limited information was available in literature.

The present study revealed that acoustic wave propagation is sensitive to variation in acoustic parameters of bone and to the presence of soft tissues. The min/max sensitivities were higher than the defect sensitivities for the receiver that was placed outside the ankle joint space (Table 2, Figure 9). The defect sensitivities were only higher than the min/max sensitivities for the receiver inside the ankle joint space (Table 3 and Figure 9). The defect sensitivities increased with the addition of Achilles tendon and skin (Table 5). The following sections will describe above drawn conclusions more extensively.

Acoustic parameters required for the computational model

The following section compares our experimentally derived values for the acoustic parameter of Achilles tendon and skin among each other and compares the experimentally determined values with those reported in literature (Table 1 and Table 6). Little information about the acoustic parameters of Achilles tendon and skin is available in literature. However, the information available is presented in Table 6. In comparison with those data, the results of our experimentally determined values for skin and Achilles tendon tissue are in agreement with the values presented in literature. Our results showed less variation than the different studies in literature. The thickness of the Achilles tendon was in the range as presented in literature. The range described in literature for the thickness of skin was very broad, and no information about the thickness of the skin of the ankle was presented in literature. The densities of skin and Achilles tendon were higher in our experiment than in literature. However, densities of both tissues were similar, as expected. The experimentally determined acoustic velocity was lower for both Achilles tendon and skin than the one given in literature. Little information about the attenuation of Achilles tendon and skin was presented in literature. However, Duck et al. (1980) report $\alpha = 1.2$ dB/cm/MHz for bovine Achilles tendon, which is similar to the mean value for the attenuation found for human Achilles tendon tissue in our experiment(27). The standard deviation for the attenuation was high in the present study. However, attenuation with a high standard deviation was found for the attenuation of bone and skin in literature also. The broad range is expected to be caused by two reasons: spatial differences within tissues and deformations of the Fourier spectra because the surfaces of the tissues were not completely flat. Fatty tissue and other irregularities were removed as accurately as possible during the dissection of the ankles however the surfaces of the tissues were not completely flat. For the determination of the attenuation the Fourier spectra of the waves that are reflected by the reflector plate and that have travelled through the sample are compared. The thickness and longitudinal velocity were calculated based on a phase shift which is less sensitive to the deformation of the signals and low variation was found.

Studies that used a similar measurement technique to determine the thickness, longitudinal velocity and attenuation used a membrane placed on top of the samples to ensure flat surfaces or used frozen samples which could be cut flat by use of a cutting machine. Because our aim was to determine the acoustic parameters of Achilles tendon and skin as closely as possible similar to in vivo conditions unfrozen samples were used. The presence of a membrane influences the material properties which reduces the reliability of the obtained acoustic parameters. The currently used measurement technique requires that the tissues lay completely flat on the reflector plate. During the current experiment this requirement could not be fulfilled due to a too weak pumping system. One Achilles tendon sample was discarded because it was not positioned rightly on the reflector plate. For the other samples we had to remove a few grid points per sample, which had marginal effect due to the large number of grid points that we used (approx. 400 grid points per skin sample, and 600 for each Achilles tendon sample). Overall, it can be concluded that the experimentally determined thickness, longitudinal velocity, attenuation and density of skin and Achilles tendon are an addition to what is currently reported in literature.

Table 6: Overview of the acoustic parameters of Achilles tendon and skin that were determined experimentally and described by literature. Acoustic parameters are presented by mean (standard deviation), abbreviations: + = bovine tendon tissue

	Experimentally determined acoustic parameters				Acoustic parameters described by literature			
	V_l (m/s)	α (dB /cm/MHz)	l (mm)	ρ (kg/m^3)	V_l (m/s)	α (dB /cm/MHz)	l (mm)	ρ (kg/m^3)
Skin	1187 (28.5) *	0.86 (0.40) *	2.5 (0.95) *	1517 (1) *	1647(104)[27, 30-32]	0.51(0.69) [30, 31, 33]	2.75(1.8)[34]	1060(42)[27, 30]
Tendon	1574 (13.5) *	1.21 (1.5) *	4.57 (1.7) *	1512 (70) *	1750*[27, 35]	1.21+[27]	6.9(36)	1060(42) [27, 37]

Acoustic wave propagation through the ankle joint space

The proposed diagnostic technique for the identification of OCDs is based on the deviation in the output signal caused by changes in the ankle joint space due to an OCD. OCDs should be detected by comparing the output signal of the ankle joint space with an OCD to a patient specific reference signal of the healthy ankle joint space, the difference between those two signals can indicate the presence of an OCD. When the proposed diagnostic technique will be applicable in the clinic, only the acoustic waves collected by the receiver outside the ankle joint space will be available for the identification of an OCD. The amplitudes of the waves collected by the receiver outside the ankle joint space were small compared to the output signals collected by the receivers placed inside the ankle joint space (middle or anterior side of the ankle joint space) (Figure 5 and Figure 6). This difference in amplitudes is expected to be caused by the difference in distance the waves have travelled before being collected by differently placed receivers. The larger the distance the more the amplitudes are affected by boundary effects. At boundaries between two different tissues the amplitude decreases due to transmission and reflection. The difference in amplitude between the receiver at the anterior and at the outside of the ankle joint space is expected to be caused by the distance between the ankle joint space and the receiver. Parts of the waves are not collected by the receiver.
The output signals of the receiver on the anterior side of the ankle joint space and the output signals of the receiver outside the ankle joint space show a trend of decreasing amplitudes (Figure 6). The receiver on the anterior and outside of the ankle joint space collected waves that have propagated

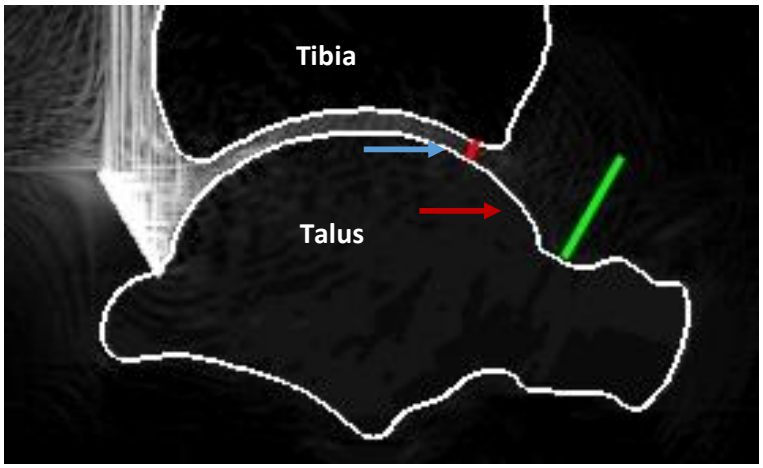

Figure 10 : Part of the waves that are collected by the receivers that were placed on the anterior and outside of the joint space have propagated through bone, this is expected to result in the decaying trend in the output signals

through the ankle joint space but also waves that have propagated through the Talus (Figure 10). The reflection and transmission effects that occur due to the interactions with bone are more present in the receivers on the anterior and outside of the ankle joint space, than in the output signals of the receiver placed at the middle or at the posterior side of the ankle joint space. It is expected that this effect results in the decreasing trend in the amplitude of the output signals.
Research on the placement of the transmitter and the frequency of the input signal should be conducted to investigate if the intensity of the acoustic waves that are collected by the receiver outside the ankle joint space can be increased.

Sensitivity analysis

The following section evaluates the min/max sensitivities compared to the defect sensitivities. A study conducted by White et al. (2010) has shown that the geometry of the ankle joint space influences acoustic wave propagation (11). However, based on our previous study we expected that the identification of OCDs is challenging because the variation caused by the natural variation in ankle joint space geometry were in the same range as the variation caused by an OCD(10). The NRMSE was higher than 1% for all sensitivities. Present study indicates that the min/max sensitivities are in the same range as the defect sensitivity for the receiver outside the ankle joint space (Table 2). However, these conclusions are based on the NRMSE and NMCC and the positioned transmitter with a frequency of 1 MHz that were used during present study. We concluded this since based on the NRMSE values the min/max sensitivities were higher than the defect sensitivities. The minimal and maximal acoustic parameters of bone resulted in acoustic waves with different amplitudes and propagating speed. These effects resulted in a change in time shift and amplitude. The time shift is similar in both healthy and defected ankle conditions. This means that the defect sensitivities are only based on a change in amplitude only. This resulted in a lower defect sensitivity than the min/max sensitivity (Figure 9). The min/max sensitivity is caused by a change in amplitude and time shift. In addition, the NMCC was found in the same range for the min/max sensitivities and the defect sensitivities. All NMCC values were close to 0.95 which indicates that the shape of the signal did not changed significantly.

Present study reveals that the defect sensitivities were similar or higher than the min/max sensitivities for the receiver in the middle of the ankle joint space (Table 3 and Figure 9). The time shift between healthy and defected ankle conditions were different, and a larger difference in amplitude was found between healthy and defected ankle conditions than for the receiver outside the joint space. This resulted in NRMSE for the defect sensitivities that were caused by changes in both time shift and amplitude. The NMCC was low which is a result of the difference in amplitudes between the health ankle condition and the condition with an OCD.

The density and the stiffness of the medium (that is described by the Lamé's constants in Equation 1) influenced the amplitude of the signal and resulted in a time shift, whereas the bulk and shear viscosity only influenced the amplitude. For all three receivers the relation between the acoustic parameters and time shift was found as represented in Table 7. Based on theory it was expected that an increase in density would lead to a lower propagating speed within the medium (represented by the + in Table 7), whereas an increased stiffness would lead to a higher propagation speed within the medium (represented by the – in Table 7). The amplitude of the situations with maximal bulk and shear viscosity decreases or stays similar to the reference situation. Whereas the amplitude of the situations with minimal bulk and shear viscosity increases or stays similar. However, the overall smallest and largest amplitudes were found for the conditions with variation in density and Lamé's constants.

Table 7: Relation between acoustic parameter and time shift versus the model of the ankle joint with mean acoustic parameters.

	ρ (Kg/m^3)		λ & μ (MPa)		η & β (Pa·s)	
	Min	Max	Min	Max	Min	Max
Time shift (μs)	-	+	+	-	0	0

The NRMSE of the bulk and shear viscosity showed a trend of being lower than the NRMSE of the density and Lamé's constants in the healthy ankle condition (Table 2). In the ankle condition with an OCD the NRMSE of the maximal bulk and shear viscosity was lower than the NRMSE values of the density and Lamé's constants**.** This could be an effect of the absence of a time shift and the fact that the bulk and shear viscosity influence the amplitude less than the density and Lamé's constants. However, when the NRMSE for the defect sensitivity are compared among the density, Lamé's constants and bulk and shear viscosity no difference is found among all acoustic parameters.
The NMCC values for the receiver in the middle, anterior and outside of the ankle joint space were close to 0.95 for the bulk and shear viscosity, this implies that the shape of the signal has not changed due to a variation in the bulk and shear viscosity (Table 2 and Table 3 and Table 4). The NMCC values for the receiver in the middle and anterior side of the ankle joint space were lower (middle: close to 0.70, anterior: close to 0.80) for the density and Lamé's constants, this implies a change in the shape of these output signals caused by the variation in the acoustic parameters. The effects on the NRMSE, NMCC, time shift and amplitude could indicate that acoustic wave propagation is less sensitive to the bulk and shear viscosity but further research is required to support this conclusion.
The mean relative difference from the mean for minimal and maximal acoustic parameter values for bone was largest (50%) for the first Lamé's constant and the shear viscosity, 30% for the second Lamé's constant and 30 % for the bulk viscosity. The density had the smallest mean relative difference (15%). However, the NMCC, NRMSE and amplitude were in the same order for all acoustic parameters. The time shift found for the Lamé's constant were higher for than for density, which can be an effect of the larger mean relative difference from the mean for this parameter. The variation in the acoustic parameters of bone that were used for the present sensitivity analysis were a result of differences in spatial location of the tissues used within the different studies (tibia or femur), differences in age of the samples, differences in measurement techniques, differences in freshness and natural variation between individuals. It is therefore expected that the variation in acoustic parameters that was used for present sensitivity analysis was broader than when the acoustic parameters will be determined under standardized circumstances for different individuals. Because the natural variation in acoustic parameters of bone between individuals is expected to be less than the variation that was used in the present sensitivity analysis

The defect sensitivities increased with the addition of Achilles tendon and skin (Table 5). This could indicate that the presence of soft tissues increases the ability of the identification of OCDs. No time shift was found so soft tissues only influence the amplitude of the propagating waves. The amplitude of the situations with the presence of Achilles tendon and skin were lower than for the reference situation. This indicates that soft tissues attenuate the acoustic waves. The addition of skin altered the shape of the outputs signal and this resulted in higher NRMSE values and lower NMCC values compared to the conditions with Achilles tendon.
This effect on the shape of the signal was clearest in the output signals of the receiver outside the ankle joint space (Figure 11 and Figure 12). Whereas the output signal from bone and Achilles tendon stays similar to the shape of the output signal of the ankle with mean acoustic parameters for bone (Figure 11 and Figure 12).

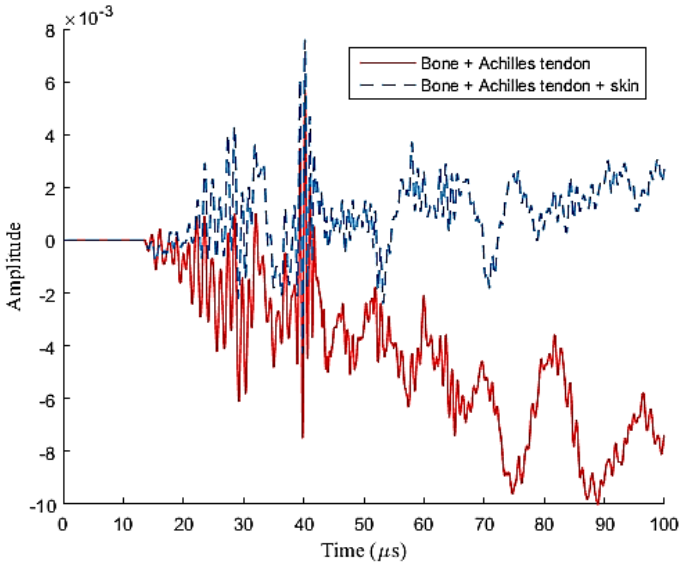

Figure 11: The output signal from the receiver on the outside of the ankle joint space for bone, Achilles tendon and skin (blue stripes) and for bone and Achilles tendon (red).

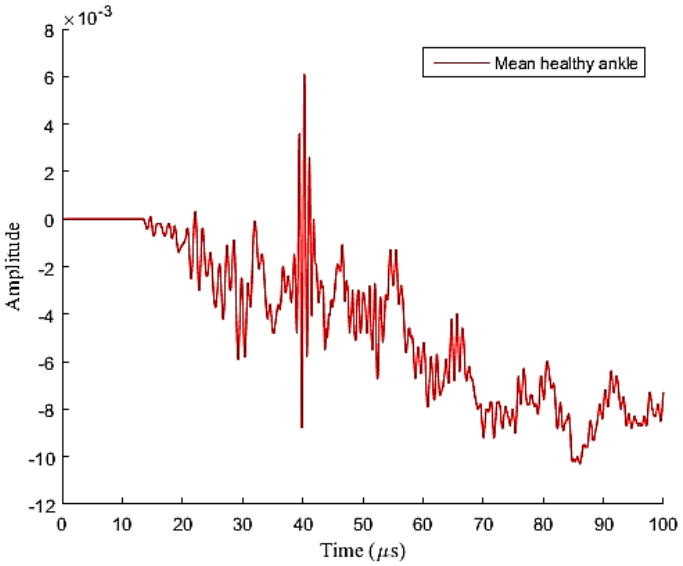

Figure 12: The output signal from the receiver on the outside of the joint space for the healthy ankle with mean acoustic parameters of bone.

Since the defect sensitivities increase with the addition of Achilles tendon and skin it is advised to take soft tissues into account when models of the ankle joint space OCD identification purposes are generated. The soft tissue sensitivities are larger than the defect sensitivities for the receiver on the outside of the ankle joint space. The effects on the amplitude and shape of the signal should not therefore not be neglected. It is advised to model soft tissues as accurately as possible and to assess the sensitivity of acoustic wave propagation and the identification of OCDs to the presence of soft tissues with various thickness. For further elaboration of the computational model of the ankle joint space the effect of a cartilage inside of the ankle joint space should be considered too, because previous studies have shown that the geometry of the ankle joint space influences acoustic wave propagation(10, 11).

One of the limitations of this study is that we assumed that bone is a homogenous material when modelled for ultrasound purposes. Since the wavelength of ultrasound is larger (a few millimetres) than the structural elements of bone, it is not assumed that this has influenced any of the results. Another limitation of the present study is that the numerical modelling was limited to two dimensions. Taking other computational studies in consideration that asses acoustic wave propagation with cartilage (38) and bone (39-41) and acoustic wave propagation through the ankle joint space of a human knee (11), we believe that two dimensional computational models are good enough. And we therefore assumed that two dimensional models can be used to assess the sensitivity of acoustic wave propagation to variation in acoustic parameters of bone and the presence of soft tissues and to indicate the feasibility of the identification of an OCD based on acoustic wave propagation.

The present study has shed some light on the sensitivity of acoustic wave propagation to variation in acoustic parameters of bone, the presence of soft tissues and the identification of OCDs. Present study reveals that for successful indication of OCDs the conditions of acoustic wave propagation (i.e. acoustic parameters and presence of soft tissues) between the healthy and defected ankle should be similar when the NRMSE and NMCC are used for the identification of OCDs. When this condition cannot be fulfilled a difference in NRMSE and NMCC can be assigned to an OCD whereas in reality this is caused by a biased estimation of the acoustic parameters or by lack or presence of soft tissues. The

precise estimation of acoustic parameters of people in vivo is challenging. However, it should be further studied whether bone density, acoustic velocity and attenuation can be measured in vivo and used for the creation of a patient specific reference model of the ankle joint space. Secondly, further research is required to indicate whether a different frequency or positioning of the transmitter will increase defect sensitivity of the receiver outside the ankle joint space. The intensity of the waves is expected to increase by placing the receiver outside the ankle joint space closer to the anterior end of the ankle joint space. However, this will not increase the possibility of the identification of OCDs when the NRMSE and NMCC are used as similarity measures. And further research should be conducted on more excessive signal processing steps which are more robust and correct for example the time shift and change in the shape of the signal for the identification of OCDs.
The proposed diagnostic technique is expected to be better for the identification of small OCDs compared to CT and MRI. OCD identification based on acoustic wave propagation consists of a compact set-up, is cost effective and non-invasive. With improved estimation of individual acoustic parameters, higher intensity of the output signals and more robust measures it is expected that identification of OCDs and their size and location can occur more accurately than currently with MRI and CT.

Conclusion

The present study indicates that acoustic wave propagation is more sensitive to variation in acoustic parameters of bone than to the presence of an OCD. The defect sensitivity increases when Achilles tendon and skin are added to the model and should therefore be incorporated in the model. A slight difference in NRMSE and NMCC, the missing time shift and the least influence on the amplitude by the bulk and shear viscosity implies that acoustic wave propagation is less sensitive to variation in viscosity than in density and Lamé's constants. It is advised that the acoustic parameters of bone and soft tissues are estimated precisely when models of the ankle joint space for OCD identification purposes are developed. Further research should be conducted on output signals with larger amplitudes (intensity) and more excessive signal processing steps. The present study confirms that the presence of an OCD influences acoustic wave propagation through the ankle joint space because a change in amplitude can be detected when the output signals from the receiver in the middle of the ankle joint space are assessed.

References

1. Reilingh M, van Bergen C, Van Dijk C. Diagnosis and treatment of osteochondral OCDs of the ankle. South Afr Orthop J. 2009;8(2):44-50.
2. Bauer R, Steiner M. Injuries in the European Union: statistics summary 2005-2007. Vienna, Eurosafe, KfV. 2009.
3. Bhosale AM, Richardson JB. Articular cartilage: structure, injuries and review of management. British medical bulletin. 2008;87(1):77-95.
4. Khan I, Gilbert S, Singhrao S, Duance V, Archer C. Cartilage integration: evaluation of the reasons for failure of integration during cartilage repair. A review. Eur Cell Mater. 2008;16:26-39.
5. Waldt S, Bruegel M, Ganter K, Kuhn V, Link T, Rummeny E, et al. Comparison of multislice CT arthrography and MR arthrography for the detection of articular cartilage lesions of the elbow. European radiology. 2005;15(4):784-91.
6. Heywood CS, Benke MT, Brindle K, Fine KM. Correlation of magnetic resonance imaging to arthroscopic findings of stability in juvenile osteochondritis dissecans. Arthroscopy: The Journal of Arthroscopic & Related Surgery. 2011;27(2):194-9.
7. Nieminen HJ, Zheng Y, Saarakkala S, Wang Q, Toyras J, Huang Y, et al. Quantitative assessment of articular cartilage using high-frequency ultrasound: research findings and diagnostic prospects. Critical Reviews™ in Biomedical Engineering. 2009;37(6).
8. Keen HI, Conaghan PG. Ultrasonography in osteoarthritis. Radiologic Clinics of North America. 2009;47(4):581-94.

9. Möller I, Bong D, Naredo E, Filippucci E, Carrasco I, Moragues C, et al. Ultrasound in the study and monitoring of osteoarthritis. Osteoarthritis and Cartilage. 2008;16:S4-S7.
10. Sarkalkan N, Loeve AJ, van Dongen KW, Tuijthof GJ, Zadpoor AA. A novel ultrasound technique for detection of osteochondral OCDs in the ankle joint: A parametric and feasibility study. Sensors. 2014;15(1):148-65.
11. White D, Evans JA, Truscott JG, Chivers RA. Modelling the propagation of ultrasound in the joint space of a human knee. Ultrasound in medicine & biology. 2010;36(10):1736-45.
12. Kaleva E, Liukkonen J, Töyräs J, Saarakkala S, Kiviranta P, Jurvelin JS. 2-d finite difference time domain model of ultrasound reflection from normal and osteoarthritic human articular cartilage surface. Ultrasonics, Ferroelectrics, and Frequency Control, IEEE Transactions on. 2010;57(4):892-9.
13. Van Dijk CN. Ankle arthroscopy: techniques developed by the Amsterdam Foot and Ankle School: Springer Science & Business; 2014.
14. Aula AS, Töyräs J, Hakulinen MA, Jurvelin JS. Effect of Bone Marrow on Acoustic Properties of Trabecular Bone - 3D Finite Difference Modeling Study. Ultrasound in Medicine & Biology. 2009;35(2):308-18.
15. Schechter R, Chaskelis H, Mignogna R, Delsanto P. Real-time parallel computation and visualization of ultrasonic pulses in solids. Science. 1994;265(5176):1188-92.
16. Szabo TL. Diagnostic ultrasound imaging: inside out: Academic Press; 2004.
17. Kino GS. Acoustic waves: devices, imaging, and analog signal processing: Prentice-Hall Englewood Cliffs, NJ; 1987.
18. MacDonald Patrick H. Continuum mechanics: PWS Publishing Company; 1995.
19. Hill CR, Bamber JC, ter Haar G. Physical principles of medical ultrasonics: Wiley Online Library; 2004.
20. Mason WP. Physical acoustics: Elsevier Science; 2013.
21. White D, Evans J, Truscott J, Chivers R. Can ultrasound propagate in the joint space of a human knee? Ultrasound in medicine & biology. 2007;33(7):1104-11.
22. Fam H, Bryant J, Kontopoulou M. Rheological properties of synovial fluids. Biorheology. 2006;44(2):59-74.
23. Keijzer L. Development of an Experimental Setup forMeasuring the Speed of Sound andAttenuation in Breast Tissue. Master's Thesis Applied Physics, TU Delft, Delft, The Netherlands. 2015.
24. Parker KJ. Ultrasonic attenuation and absorption in liver tissue. Ultrasound in medicine & biology. 1983;9(4):363-9.
25. DiResta G, Lee J, Lau N, Ali F, Galicich J, Arbit E. Measurement of brain tissue density using pycnometry. Brain Edema VIII: Springer; 1990. p. 34-6.
26. Sebaa N, Fellah ZEA, Fellah M, Ogam E, Wirgin A, Mitri F, et al. Ultrasonic characterization of human cancellous bone using the Biot theory: Inverse problem. The Journal of the Acoustical Society of America. 2006;120(4):1816-24.
27. Duck FA. Physical properties of tissues: a comprehensive reference book: Academic press; 2013.
28. Goss S, Johnston R, Dunn F. Compilation of empirical ultrasonic properties of mammalian tissues. II. The Journal of the Acoustical Society of America. 1980;68(1):93-108.
29. Droin P, Berger G, Laugier P. Velocity dispersion of acoustic waves in cancellous bone. Ultrasonics, Ferroelectrics, and Frequency Control, IEEE Transactions on. 1998;45(3):581-92.
30. Yongchen S, Yanwu D, Jie T, Zhensheng T, editors. Ultrasonic propagation parameters in human tissues. IEEE 1986 Ultrasonics Symposium; 1986: IEEE.
31. Goss S, Johnston R, Dunn F. Comprehensive compilation of empirical ultrasonic properties of mammalian tissues. The Journal of the Acoustical Society of America. 1978;64(2):423-57.
32. Mast TD. Empirical relationships between acoustic parameters in human soft tissues. Acoustics Research Letters Online. 2000;1(2):37-42.

33. Moran C, Bush N, Bamber J. Ultrasonic propagation properties of excised human skin. Ultrasound in medicine & biology. 1995;21(9):1177-90.
34. Griffiths C, Russman AN, Majmudar G, Singer RS, Hamilton TA, Voorhees JJ. Restoration of collagen formation in photodamaged human skin by tretinoin (retinoic acid). New England Journal of Medicine. 1993;329(8):530-5.
35. Goss S, O'Brien Jr W. Direct ultrasonic velocity measurements of mammalian collagen threads. The Journal of the Acoustical Society of America. 1979;65(2):507-11.
36. Koivunen-Niemelä T, Parkkola K. Anatomy of the Achilles tendon (tendo calcaneus) with respect to tendon thickness measurements. Surgical and radiologic anatomy. 1995;17(3):263-8.
37. Kuo P-L, Li P-C, Li M-L. Elastic properties of tendon measured by two different approaches. Ultrasound in medicine & biology. 2001;27(9):1275-84.
38. Kaleva E, Liukkonen J, Toyras J, Saarakkala S, Kiviranta P, Jurvelin JS. 2-D finite difference time domain model of ultrasound reflection from normal and osteoarthritic human articular cartilage surface. Ultrasonics, Ferroelectrics and Frequency Control, IEEE Transactions on. 2010;57(4):892-9.
39. Bossy E, Talmant M, Laugier P. Effect of bone cortical thickness on velocity measurements using ultrasonic axial transmission: A 2D simulation study. The Journal of the Acoustical Society of America. 2002;112(1):297-307.
40. Dodd S, Miles A, Gheduzzi S, Humphrey V, Cunningham J. Modelling the effects of different fracture geometries and healing stages on ultrasound signal loss across a long bone fracture. Computer methods in biomechanics and biomedical engineering. 2007;10(5):371-5.
41. Protopappas VC, Fotiadis DI, Malizos KN. Guided ultrasound wave propagation in intact and healing long bones. Ultrasound in medicine & biology. 2006;32(5):693-708.

Appendix A. Protocol dissection human cadaver ankles at the Amsterdam Medical Center

Version 1.0
6 - 6 - 2015

R.M. Oosting
Department of Biomechanical Engineering, TU Delft
Email: roosmariekeoosting@gmail.com
0630715292

Gwen Vuurberg
Department of Orthopaedic Surgery, AMC
Email:g.vuurberg@amc.uva.nl

Elise Buiter
Department of Biomechanical Engineering, TU Delft
Email: elisebuiter@gmail.com

Julius Zonneveld
Department of Biomechanical Engineering, TU Delft
Email:jw.zonneveld@gmail.com

Introduction

The acoustic parameters of the soft tissues present in the ankle joint space are not extensively described by literature. An experiment to determine the density, thickness, acoustic velocity and attenuation will be therefore conducted. The main interest of our study is on the skin and Achilles tendon, but other tendon tissue was dissected as well for usage in future studies.

General time line

Time & Date	Task	Participant
Friday 3 July 2015	Preparation ankles @ AMC	Roos
Monday 6 July 2015	Transport ankles from mortuary to pathology section in the AMC	Roos, Gwen, Elise and Julius
Monday 6 July 2015	Dissection of 3 ankles	Roos, Gwen, Elise and Julius
Monday 6 July 2015	Preparation ankles for 8 July @ AMC	Roos
Wednesday 8 July	Transport ankles from mortuary to pathology	Roos, Gwen, Elise
Wednesday 8 July	Dissection of 8 ankles	Roos, Gwen, Elise

Objective

The objective of the dissection of the human cadaver ankles was to obtain as much intact human soft tissues from the ankles as possible. The samples are required for an experiment to determine the acoustic parameters of the soft tissues for ultrasound research purposes.

Responsibilities

Thijs: Access to the pathology section at the AMC
Gwen: Sample selection from the human cadaver ankles
Elise and Julius: Dissection of the ankles
Roos: selection of the samples and preparing the bags for storage

Dissection

Preparation of the ankle:

- Remove and collect the skin from the ankle
- Remove and collect the Achilles tendon from the ankle
- Remove (if intact) other tendons or ligament structures
- Carefully remove tibia, talus and calcaneus from joint
- Remove all excess material
- Check the cartilage surface for undamaged cartilage, if present collect

Collection and storage of the specimen:

- Make photo of specimens from the top
- Bag specimens
- Write name specimen, cadaver # on bag
- Write name specimen, cadaver # and photo number on form

Specimen

11 cadaver ankles that were frozen and defrosted 3 times (age, sex and cause of death unknown) were used for the dissection of the samples. The ankles were used for the Foot and Ankle Course organised by the AMC in June. Several surgical procedures were performed and practised on these ankles.

Equipment

	Parts	Location	Responsibility
☐	# Specimens	AMC mortuary freezer	ECB
☐	Closable bags	AMC	RO
☐	Gloves	AMC	RO
☐	Markers	AMC/TUD	ECB&RO
☐	Print out of protocol	TUD	ECB
☐	Camera	AMC	RO
☐	Print out forms	AMC	RO

☐	Lab coats	AMC	RO

Results

Table 8 : Tissue samples that were dissected on 6 July 2015.

Sample number	Cadaver	Tissue
1	1	Achilles Tendon
2	1	Peroneus Brevus
3	1	Peroneus Longus
4	2	Peroneus Brevus
5	2	Peroneus Longus
6	1	Digitorum Longus
7	2	Skin
8	1	Hallicus longus
9	1	Ligament
10	1	Tibialis Posterior
11	2	Flexor. Digitorum Longus
12	1	Flexor digitorum longus
13	2	Tibialis Posterior
14	2	Tibialis Anterior
15	2	Extensor complex
16		
17	3	Achilles Tendon
18	3	Tibialis anterior
19	3	Extensor hallicus longus
20	3	Tibialis posterior
21	3	Flexor hallicus longus
22	3	Peroneus Brevus
23	3	Extensor digitorum longus

Table 9 Tissue samples that were dissected on 8 juli 2015.

Sample number	Cadaver	Tissue
1	4	Achilles Tendon
2	5	Achilles Tendon
3	6	Achilles Tendon
4	4	Skin
5	6	Skin
6	5	Peroneus brevus
7	5	Peroneus longus
8	5	Skin
9	4	Peroneus brevus
10	4	Peroneus longus
11	6	Peroneus brevus
12	6	Peroneus longus
13	7	Skin
14	5	Anterior kapsel
15	4	Flexor hallicus longus
16	4	Tibialis posterior
17	4	Flexor digitorum longus
18	5	Flexor hallicus longus
19	5	Tibialis posterior
20	5	Flexor digitorum longus
21	4	Extensor digitorum longus
22	4	Extensor hallicus longus
23	4	Tibialis posterior
24	6	Tibialis anterior
25	6	Extensor hallicus longus
26	5	Extensor digitorum longus
27	5	Extensor hallicus longus
28	5	Tibialis anterior
29	6	Extensor digitorum longus
30	5	ATFL
31	7	Achilles Tendon
32	7	Skin
33	6	Flexor hallicus longus
34	6	Flexor digitorum longus
35	6	Tibialis posterior
36	7	Extensor digitorum longus
37	7	Tibialis posterior
38	7	Flexor digitorum longus
39	7	Extensor hallicus longus
40	7	Tibialis anterior
41	7	Peroneus longus

42	7	Peroneus brevus
43	7	Calcaneus ligament
44	5	Sinus tarsi
45	8	Achilles Tendon
46	9	Achilles Tendon
47	10	Skin
48	9	Peroneus brevus
49	8	Peroneus longus
50	8	Peroneus brevus
51	9	Skin
52	8	Extersorum retinacium
53	8	Extensor digitorum
54	10	Skin
55	8	Tibialis anterior
56	10	Achilles tendon
57	9	Extensorum retinacum
58	9	Peroneus longus
59	9	Tibialis anterior
60	9	Extensor digitorum longus
61	9	Extensor hallicus longus
62	8	Flexor digitorum longus
63	8	Tibialis posterior
64	8	Flexor hallicus longus
65	9	Flexor digitorum longus
66	9	Flexor hallicus longus
67	9	Tibialis posterior
68	10	Extensor hallicus longus
69	10	Extensor digitorum longus
70	10	Peroneus brevus
71	10	Peroneus longus
72	10	Tibialis anterior
73	10	Flexor hallicus longus
74	10	Flexor digitorum longus
75	10	Tibialis posterior
76	11	Achilles Tendon
77	11	Flexor digitorum longus
78	11	Tibialis posterior
79	11	Flexor hallicus longus
80	11	Extensor hallicus longus
81	11	Extensor digitorum longus
82	11	Tibialis anterior
83	11	Peroneus brevus

Appendix B. Measurement of the acoustic parameters of human cadaver tissues of the ankle joint space.

Version 2
31-8 -2015

R.M. Oosting
Department of Biomechanical Engineering, TU Delft
Email: roosmariekeoosting@gmail.com
0630715292

Lana Keijzer
Department of Imaging Physics TU Delft
Email: lana.keijzer@gmail.com
0634842208

Nick Stigter
Department of Imaging Physics TU Delft
Email:nickstiger@hotmail.com
06 13241848

M. Stijntjes MSc
Department of Biomechanical Engineering, TU Delft
Email: m.stijntjes@tudelft.nl
0633937616

Dr. Koen W.A. van Dongen
Department of Imaging Physics, TU Delft
Email: K.W.A.vanDongen@TUDelft.nl

G.J.M. Tuijthof MSc PhD
Department of Biomechanical Engineering, TU Delft
Department of Orthopaedic Surgery, AMC
Email: g.j.m.tuijthof@tudelft.nl

Dr. Daniel Martijn de Bruin, PhD, MSc
Academic Medical Center, Amsterdam
Research Associate - Department of Biomedical Engineering & Physics
Email: d.m.debruin@amc.uva.nl

Gwen Vuurberg
Department of Orthopaedic Surgery, AMC
Email:g.vuurberg@amc.uva.nl

Anna Basiuras
Department of biomedical engineering, TU Delft
Email: anna.basiuras@gmail.com

Protocols

This study includes 2 protocols:

- Protocol A: Measurement of the acoustic velocity (c), attenuation (α) and thickness(l) of the samples by the use of the Marco scanner
- Protocol B: Measurement of the density (ρ) by the use of pycnometers

General timeline

Time & Date	Task	Participant
Friday	Preparation measurements @ TU DELFT	Lana, Nick, Marjon & Roos
Beginning sept 2015 (day 1)	Transport set – ups to AMC	Lana, Nick, Marjon & Roos
Beginning sept 2015(day 1)	Installation set – ups AMC	Lana, Nick, Roos
Beginning sept 2015(day 2)	Measurements @ AMC	Lana, Nick, Roos, Anna, Marjon
Beginning sept 2015(day 3)	Cleaning measurements setups at TU delft	Lana, Nick, Roos

Objective

The objective of this study is to measure the density (ρ), thickness(l), acoustic velocity(c) and attenuation(α) of human Achilles Tendon, extensor digitorum longus, extensor hallicus longus, peroneus brevus and skin tissue.

Description of specimen

Samples of 11 human cadaver ankles will be used. Each sample is stored separately within a plastic zip bag. A list of the samples that will be measured can be found in Appendix B. The samples are stored in the mortuary of the AMC in Amsterdam.

Responsibilities before experiments

Transport of the Macro scanner to AMC from TU Delft: Roos, Nick, Lana & Marjon
Transport of density measurement set up: Lana, Nick, Roos & Marjon
Reserve a room for measurements: Roos
Specimen collection from the mortuary at the AMC: Roos, Gwen
Preparing excel files to fill in all obtained values: Roos

Responsibilities during experiments

Access to the room: Roos
Preparations macro scanner: Roos, Lana
Preparations density measurement set up: Nick
Specimen collection macro scanner: Marjon
Specimen collection density measurements: Anna
Measuring acoustic parameters: Lana, Roos
Measuring density: Nick

Protocol A. Measurements Macro scanner

Room: L0 - 243

Access: Roos, Daniel de Bruin
Participants: Lana, Roos, Marjon

Supplies

At AMC

Check	What	Where	Who
☐	Samples	Mortuary AMC	Roos, Gwen
☐	Ruler(3X)	AMC	Roos
☐	Extension cord	AMC	Roos
☐	Paper towels	AMC	Roos
☐	Gloves (xl, l, s)	AMC	Roos
☐	Surgical gowns(6X)	AMC	Roos, Gwen
☐	4 x containers/buckets for the collection of samples		
☐	Soap	AMC	Roos
☐	Table cover (3x)	AMC	Roos
☐	1 X small bucket for water removal from the tank	AMC	Roos
☐	Printed protocol (3x)	AMC	Roos
☐	Printed excel sheet(3x)	AMC	Roos
☐	Pens	AMC	Roos

Bringing from Delft

Check	What	Where	Who
☐	Laptop + adaptor + connecting device for motor	TU Delft	Lana
☐	Transducer (Olympus, United states of America) + holder +reserve transducer	TU Delft	Lana
☐	Oscilloscope (Agilent DSO7054A, KeySight technologies, Amsterdam, The Netherlands) + electricity cable + USB cable	TU Delft	Lana
☐	Aquarium + pump system + device to fix position of pump	TU Delft	Lana
☐	Motor measurement system + axes	TU Delft	Lana
☐	Webcam + long cable	TU Delft	Lana

☐	Temperature measurement set up (heater, temperature controller, temperature measurement device + stand)	TU Delft	Lana
☐	Metal block +reserve metal block	TU Delft	Lana
☐	Phosphate- buffered saline 30 L	TU Delft	Lana , Nick
☐	Cover to transport the aquarium	TU Delft	Roos, Lana
☐	Tie rips	TU Delft	Roos
☐	Duct tape	TU Delft	Roos
☐	Elastic bands	TU Delft	Roos
☐	Pulser/receiver device (Panametrics NDT 5077PR, Olympus, United states of America) + electricity cable + 2 output cables + T splitter	TU Delft	Lana
☐	'waterpas'	TU Delft	Roos
☐	USB stick to save overload of data	TU Delft	Roos
☐	USB stick with all codes (as back up)	TU Delft	Lana
☐	'tang'	TU Delft	Lana
☐	Adapter for COM ports XY-system	TU Delft	Lana
☐	3 cables to connect scope and pulser	TU Delft	Lana
☐	T-splitter	TU Delft	Lana
☐	Cover for aquarium	TU Delft	Lana
☐	XY-raster, stepping motor	TU Delft	Lana
☐	Elastic bands	TU Delft	Lana
☐	screwdriver	TU Delft	Roos

Timeline

Time & Date	Task	Participant
Beginning sept 2015 (day 1)	Preparation measurements set ups @ AMC Specimen collection (Roos) from freezer mortuary to freezer in the biomedical engineering lab.	Lana, Nick, Marjon & Roos
Morning day 2 @ AMC	Test run	Lana, Nick, Roos, Anna, Marjon
Afternoon day 2 @ AMC	Measure all specimens Prepare set up for transport	Lana, Nick, Roos, Anna, Marjon

Preparing experimental set up

Preparing set up:

1. Connect the stepping motor to the laptop; com 1: x axis, com 2: y-axis, oscilloscope and webcam to computer and connect the oscilloscope with the pulser/receiver unit

2. Connect the oscilloscope to the computer by the usb cable and connect the machine to a power point
3. Connect the Webcam to the computer by a usb cable
4. Connect the pulser/receiver to the oscilloscope ant to a power point
5. Connect the thermocouple to the thermometer and the heater a to a power point

All above mention steps are also visualized in the picture below!!

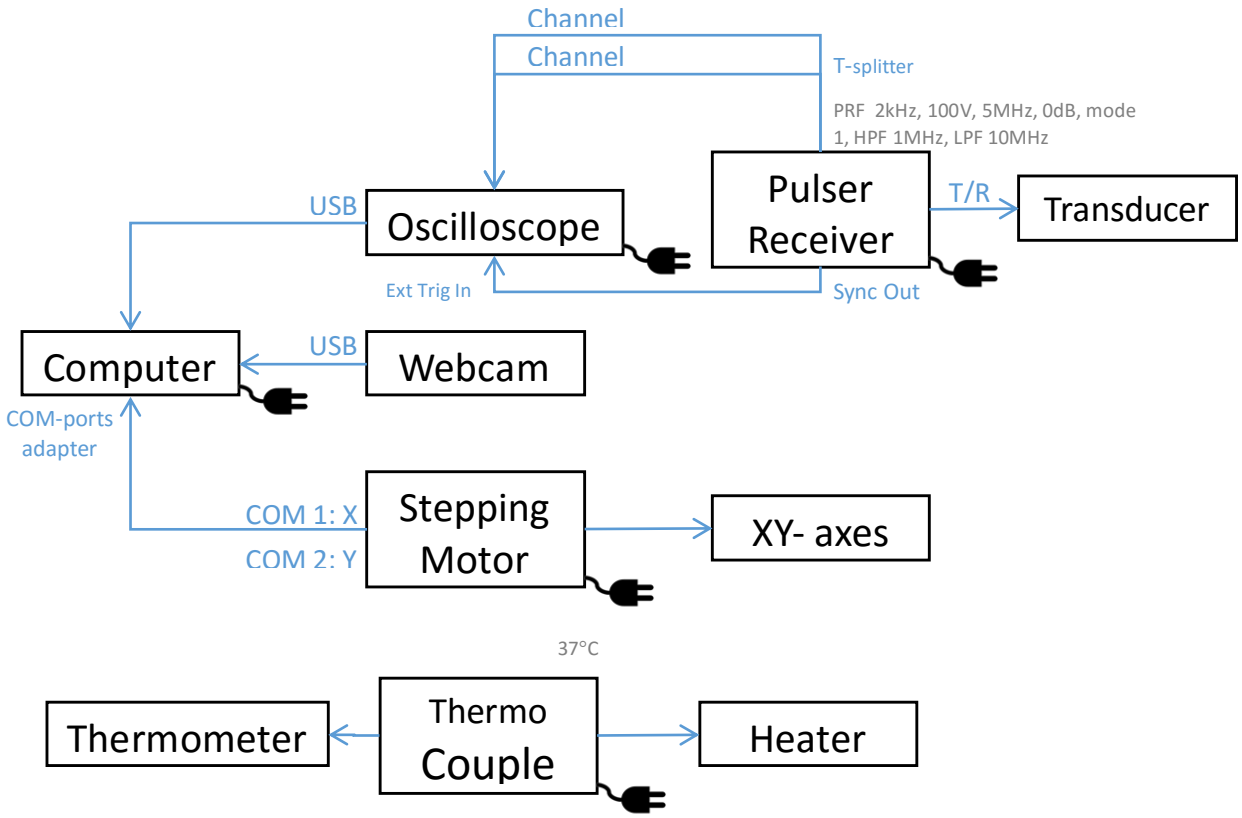

6. Turn computer on and open matlab
7. Make sure that no air bubbles are present in the pumping system, remove them with you hand if present
8. Turn the wave generator on (only when in the water)
9. Turn the oscilloscope on

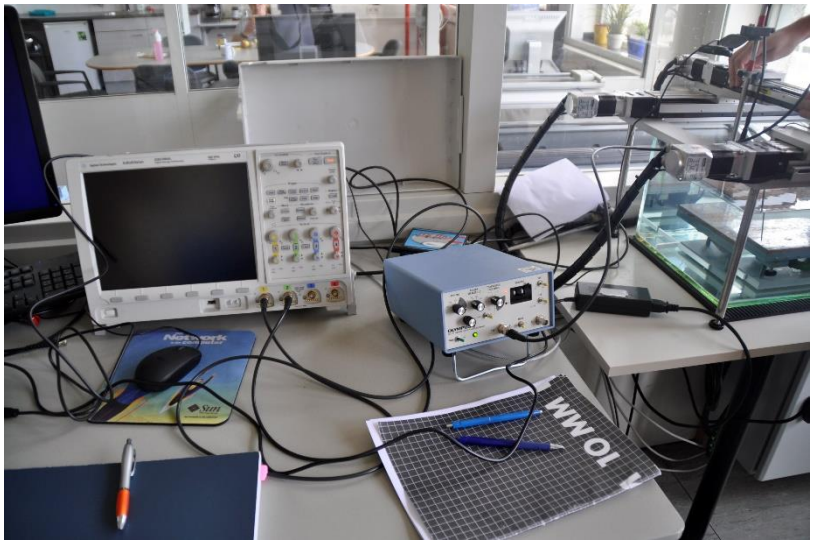

10. Make sure that the plate is exactly horizontal by checking if the signal is in the middle on the oscilloscope screen and by comparing arrival times on the oscilloscope
11. Take a picture with the webcam to check
12. Put the heater on and set to 37 degrees and wait until the water tank is indeed 37 degrees!

13. Make sure that a second channel is present on the oscilloscope for the reflection of the signal on top, this can be done by using the voltage button from channel two on the front side of the oscilloscope.

Place a sample on the plate in the aquarium:

1. Place the piece of metal next to the sample to calculate the speed of sound of water (see picture below)

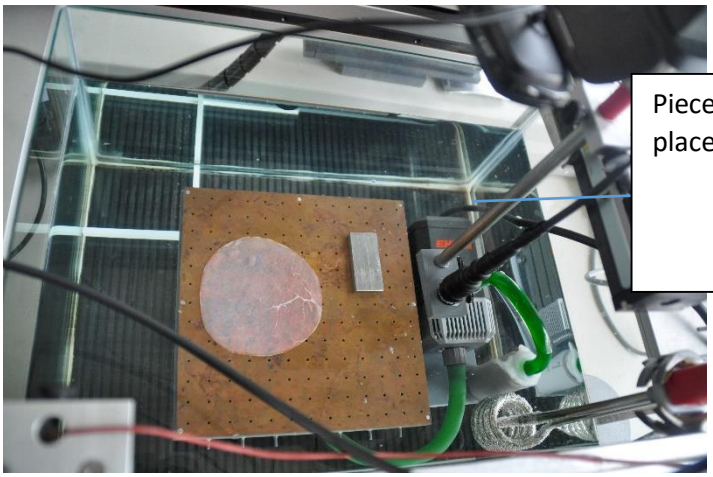

2. Adjust the scale of the second channel, make sure that both signals fit in the screen
3. Check if the offset stays in the screen

Measurements

Specimen:

4. Check excel file 'Macro scanner measurements' for the correct sample, cadaver number and name of the sample
5. Collect first sample from the plastic zipper bags
6. Measure the entire length of the tendon with the ruler and determine the middle. Cut out a piece of 5 cm that is exactly in the middle of the tendon.
7. For skin: Cut out a piece of 5 cm x 5cm

Start measurement with the Macro scanner:

8. Change measurement number in the Matlabfile ‘step_measure.m’. Very important!
9. Adjust settings of oscilloscope channel 1. Make sure that offset stays appropriate during auto-scaling. Enter the time shift, time step size, step size y axis in the ‘step_measure.m’ file. (can be read from oscilloscope)
10. Adjust settings of oscilloscope channel 2. Enter the time shift, time step size, step size y axis in the ‘step_measure.m’ file.
11. Choose number of steps and rows and choose step-size. Enter these settings in the ‘step_measure.m’ file.

12. Turn the motor of the measurement machine
12. Run the script ‘serialdrivey’
13. Change com1 into com2
14. Open script ‘step_measure.m’.
15. Enter step size in the x direction (set to 2 mm for these measurements)
16. Enter how many rows in the y direction will be scanned, this can be determined by calculating the number of points the sample covers on the metal plate on which the specimen is placed.
17. Run the script to start the measurement

Check if signal is valid, this is done by monitoring the matlab screen which should have printed ‘signal is valid’ for each measurement point. If the signal is not valid, the measurement should be stopped (Ctrl + C) and started again. An invalid signal can be caused by a fault in step 2 or 3 by that should be performed after the placement of a sample on the plate in the aquarium.

Run reference scan:

18. Remove the sample and block from the reflector
19. Run script ‘step_measure.m’ and do not change the settings of the oscilloscope
20. Check if the signal is valid, this can be done by checking the operation screen in matlab, there ‘signal is valid ‘should be printed for each measurement points

End measurement:

21. Turn the motor off in between measurements, this is an important step because the set up will become too hot otherwise.
22. Place sample back in the right zipper bag so it can be used again for the density measurements.
23. Make sure that the zipper bag is placed in the right collection container for further use.

Repeat steps 1 under placement of a sample into the aquarium till 22 until you have finished measuring all samples as indicated in the .xls file.

Final measurement:

1. Turn of the oscilloscope
2. Turn of the transducer
3. Turn of motor
4. Turn of the heater (Take care: it stays hot)

Outcome parameters

Outcomes of the measurements

1. Speed of sound of the background medium
2. Speed of sound of the sample
3. Thickness of the sample
4. Attenuation coefficient of the sample

The expected end product of the measurements are the thickness, speed of sound and attenuation in each sample. This will be reported in a table that has the following form.

Sample	Thickness	Speed of sound	Attenuation

Three matlab scripts will be used for the data processing:

- SOS_BLOCK.m to calculate the speed of sound in the background medium.
- ProcessingData_dikte2.m to determine the thickness of the sample which is needed for the calculation of the speed of sound of the sample.
- ProcessingData_sos_att2.m to calculate the speed of sound by and the frequency dependent attenuation.

Data Processing

SOS_BLOCK.m – Speed of Sound in Background Medium

1. Adjust measurement number and variables.
2. Check thresholds to select pulses reflected on block.
3. Adjust settings to cut reference pulse. (start_cut and end_cut)
4. Run total script and write down the measured average speed of sound in background medium.

ProcessingData_dikte2.m – Sample Thickness

1. Adjust measurement numbers, variables and speed of sound in background medium calculated with SOS_BLOCK.m.
2. Check thresholds to select pulses reflected on reflector. (start_cut and end_cut)
3. Adjust the threshold value to select the correct arrival times t1. For example: 0.6 max (absolute correlation).
4. Run total script. Sample thickness is saved automatically.

ProcessingData_sos_att2.m – Speed of Sound and Frequency Dependent Attenuation

1. Adjust measurement numbers, variables and speed of sound in background medium calculated with SOS_BLOCK.m.
2. Adjust settings to cut reference pulse. (start_cut and end_cut)
3. Adjust thresholds to calculate average speed of sound and statistical uncertainty. (threshold sample thickness and range of speed of sound)
4. Adjust width_pulse for windows that select the pulses.
5. Choose desired fitting method for the frequency dependent attenuation.
6. Adjust the frequency range of the fittings, by selecting the -6dB range of the reference spectra.
7. Adjust constraints of fitting variables.
8. Adjust thresholds to calculate average fitting variables. (range of speed of sound and optional the range of fitting variables)

Protocol B. Measurements of the density

Access: Roos, Daniel de Bruin
Participants: Nick, Maria

Supplies

At AMC

Check	What	Where	Who
☐	Paper towels	AMC	Roos
☐	Gloves	AMC	Roos
☐	Surgical gowns	AMC	Roos
☐	Extra table from G4 to place set ups on	AMC	Roos

Bringing from Delft

Check	What	Where	Who
☐	3 x pycnometers	TU Delft	Nick
☐	Balance	TU Delft	Nick
☐	3 x pipet	TU Delft	Nick
☐	Box pipet points	TU Delft	Nick
☐	PBS	TU Delft	Nick
☐	Pincet	TU Delft	Nick
☐	Box for balance	TU Delft	Nick

Timeline

Time & Date	Task	Participant
Beginning sept 2015 (day 1)	Preparation measurements set up@ AMC	Nick
Morning day 2 @ AMC	Test run	Nick, Anna
Afternoon day 2 @ AMC	Measure specimens Prepare set up for transport	Nick, Anna

Preparing experimental set up

Preparing set up:

1. Turn the balance on
2. Set the balance in the most accurate setting the right button on the balance (see picture below)

Measurements

Specimen

1. Check excel file ‘density measurements’ for the correct sample, cadaver number and name of the sample
2. Collect first sample from the plastic zipper bags
3. Take a picture and write the picture number down in the excel file
4. Make sure that the sample is already tested in experiment A.
5. Cut the specimen in small pieces.

Measurements:

1. Measure the empty pycnometers

2. Divide the pieces over the three pycnometers (do not fill the pycnometer above the line drawn on the pycnometers in white)
3. Enter in excel how many samples are in each pycnometer (1 = biggest, 2 = middle, 3 = smallest pycnometer)

4. Measure the weight of pycnometers with samples and write the weight down in the excel file
5. Fill the entire pycnometer with PBS by the use of a pipet
6. Dry the pycnometer on the outside to remove all the PBS (This will influence the weight that is measured)
7. Measure pycnometer with PBS + sample and write the weight down in the excel file
8. Take out the specimen and put back into the right zipper bag
9. Measure the pycnometer only filled with PBS

End measurement:

1. Make sure that the neck of the pycnometer is dry before starting the next measurement.
2. Place specimen back in the right zipper bag so it can be stored again (and/or throw it away in blue buckets from the mortuary)

Outcome parameters

1. Weight of the empty pycnometer(m1)
2. Weight of the pycnometer with sample (m2)
3. Weight of the pycnometer with sample and pbs(m3)
4. Weight of the pycnometer with pbs (m4)

Expected end product of the performed measurements

The expected end product of the measurements is the density of each sample. This will be reported in a table that has the following form.

Sample	Density

Appendix B-1. Cleaning Macro scanner set- up

Cleaning:

1. Remove the movable parts of the transducer
2. Make sure everything is cooled down
3. Remove all PBS
4. Take out the heater
5. Take out the plate
6. Take out the pump
7. Clean everything with water and soap and dry
8. Put the pump overnight in soap
9. Take the pump out after 24 h and put in a bad with only water to remove all the soap
10. Take the pump out after 24 h and make sure it can dry safely

Appendix B-2. Cleaning Pycnometers

Cleaning:

1. Make sure that the pycnometers are empty
2. Clean with water and soap
3. Make sure that the pycnometers are dry before they will be used again

Appendix B-3. List of specimen

Sample number	Cadaver	Tissue
1	4	Achilles Tendon
2	5	Achilles Tendon
3	6	Achilles Tendon
31	7	Achilles Tendon
45	8	Achilles Tendon
46	9	Achilles Tendon
56	10	Achilles tendon
76	11	Achilles Tendon
53	8	Extensor digitorum longus
21	4	Extensor digitorum longus
26	5	Extensor digitorum longus
29	6	Extensor digitorum longus
36	7	Extensor digitorum longus
60	9	Extensor digitorum longus
69	10	Extensor digitorum longus
81	11	Extensor digitorum longus
22	4	Extensor hallicus longus
25	6	Extensor hallicus longus
27	5	Extensor hallicus longus
61	9	Extensor hallicus longus
68	10	Extensor hallicus longus
80	11	Extensor hallicus longus
39	7	Extensor hallicus longus
6	5	Peroneus brevus
9	4	Peroneus brevus
11	6	Peroneus brevus
48	9	Peroneus brevus
70	10	Peroneus brevus
83	11	Peroneus brevus
42	7	Peroneus brevus
50	8	Peroneus brevus
4	4	Skin
5	6	Skin
8	5	Skin
13	7	Skin
32	7	Skin
47	10	Skin
51	9	Skin
54	10	Skin

Appendix C. Data processing experiment: Acoustic parameters of skin, Achilles tendon and the extensor digitorum longus.

The steps that were performed for the data processing of the thickness (l), longitudinal velocity (V_l), attenuation (α) and density (ρ) are described in present Appendix. The data processing steps were computed in Matlab R2015b (*The MathWorks, Inc., Natick, MA, USA*).

Pulse Echo Method (Marcos canner)

The thickness(l), longitudinal velocity within the sample(V_{sample}) and attenuation(α) of skin and Achilles tendon were determined by the use of the Macro scanner (*Set-up build by Lana Keijzer and Dr.Koen W.A van Dongen, Applied physics, TU Delft, The Netherlands, 2015*) that is based on the pulse-echo method (1). The pulses obtained from tissue samples that were placed on the reflector plate were compared to a reference scan without tissue samples similar as described by Parker et al.(1983)(1). One spherically focused transducer with centre frequency 5 MHz and focal distance 38 mm (Olympus, United states of America) was used that both acted as source and receiver. The pulses were generated by a square wave pulser and receiver unit (Panametrics-NDT 5077PR Olympus, *Massachusetts,* United States of America). Pulses were emitted with a pulse repetition frequency of 2 kHz and a pulser voltage of 100 V. A high pass filter of 1 MHz and a low pass filter of 10 MHz were used to filter the output. The transmitted waves were sent through the sample and reflected by a reflector plate aligned perpendicular to the transducer (Figure 12). The signals were read out by an oscilloscope with a sampling rate of 50 MHz (Agilent DSO7054A, KeySight technologies, Amsterdam, The Netherlands). Phosphate buffered saline(PBS) was used as background medium to mimic in vivo conditions. The measurements were performed at 37℃.

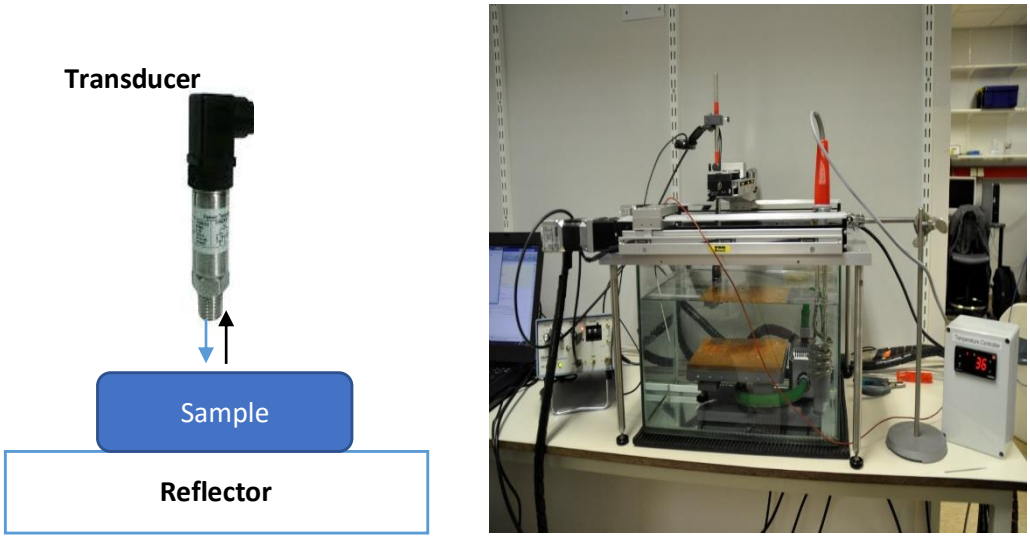

Figure 12 A transducer that acted as source (transmitted acoustic waves, blue arrow) and receiver (collected acoustic waves, black arrow) was placed above the samples that were placed on top of the reflector plate. Right: the whole set-up, that consist of a water tank (with PBS), the transducer and reflector plate, a heating system and a motor system that was used to scan the entire surface of the samples.

Longitudinal velocity in the sample (V_{Sample})

To obtain the longitudinal velocity within each sample (V_{sample}) the reflection pulse from the reflector plate (t_0), the reflection pulse from the sample (t_1) and the reflection plate and the sample(t_2) were required (**Fout! Verwijzingsbron niet gevonden.**,Figure 14).

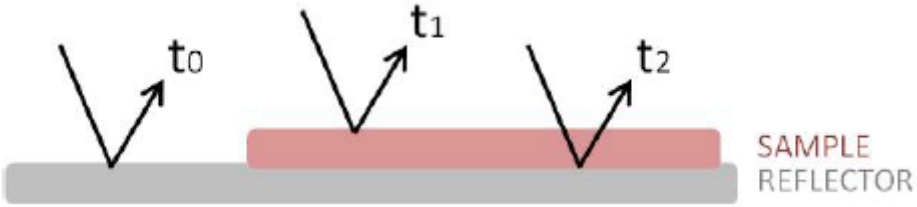

Figure 13 :Reflection pulses from the sample and reflection plate (Image made by Lana Keijzer, Applied physics, TU Delft, The Netherlands, 2015)

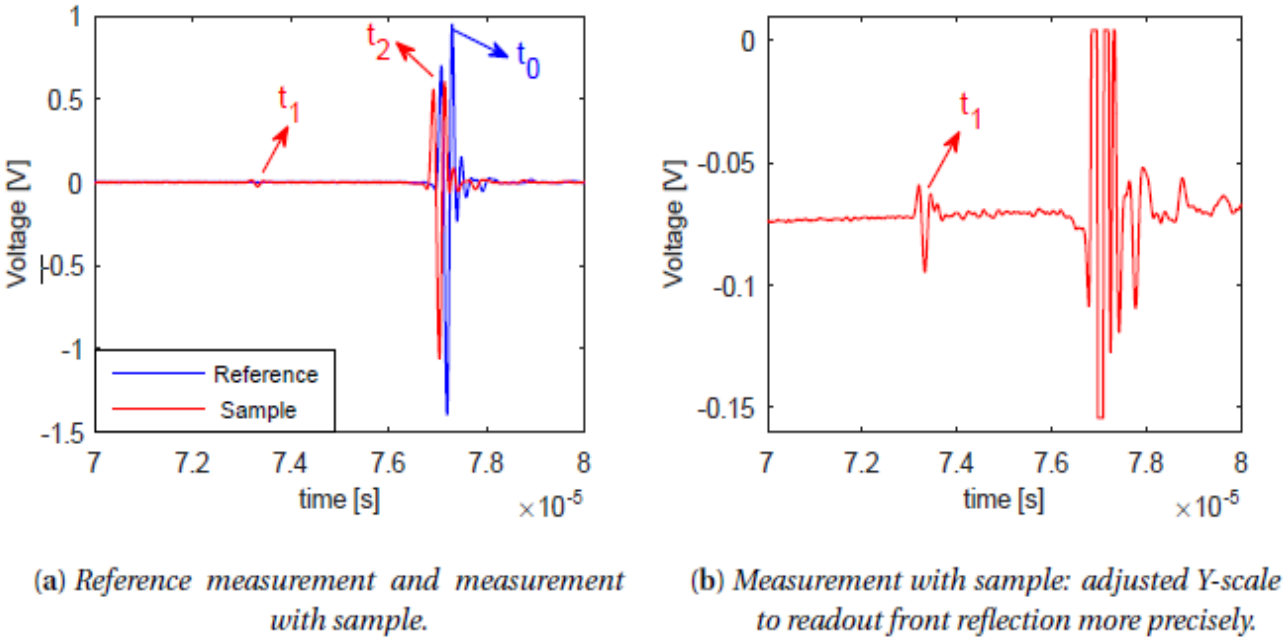

(a) *Reference measurement and measurement with sample.*

(b) *Measurement with sample: adjusted Y-scale to readout front reflection more precisely.*

Figure 14: Reflection pulses (t0, t1, t2) from the sample and reference signal.

The longitudinal velocity in the sample was described by Equation 7.

$$V_l\,(x,y) = \frac{2l\,(x,y)V_{background}}{V_{background}(t_2(x,y)-t_0)+2l\,(x,y)} \qquad \text{(Equation 7)}$$

l (x, y) = the thickness per grid point.

To obtain the longitudinal velocity in the samples (V_{sample}) first the longitudinal velocity in the background medium ($V_{background}$) was determined. Second, the thickness ($l(x,y)$) at each grid point was determined and third, the longitudinal velocity in the sample ($V_{sample(x,y)}$) was determined per grid point.

Longitudinal velocity background medium

The longitudinal velocity in the background medium ($V_{background}$) is required for Equation 7 and can be determined by Equation 8. Therefore, a metal block with known height ($h = 9.93$ mm) was placed next to the samples.

$$V_{background} = \frac{2h}{t_0} \qquad \text{(Equation 8)}$$

The longitudinal velocity of the background medium ($V_{background}$) was determined by the use of the Matlab script SOS_BLOCK.m (*Written by Lana Keijzer, Applied physics, T U Delft, The Netherlands, 2015)*.

First the thickness (l) at each grid point was guessed by the use of an initial guess of longitudinal velocity within the background medium ($V_{background}$)(1500 m/s for PBS). The height of the metal block was known on forehand (h= 9.93 mm), therefore the grid points with a height between 9 mm and 14 mm were selected to select the block position (Figure 15).

The arrival times of the reflected pulses of each grid points of the block (t_0) were compared with the reference measurement. The reflected pulses deform, in particular the front reflections (t_1) of the samples, therefore the cross correlation between the reference pulse (t_0) and the reflected pulse (t_1) was computed (Figure 15). The time value with the highest absolute correlation was selected (Figure 15). This method was combined with a method of zero-padding with a factor of 2 in the frequency domain to increase the sampling rate in the time domain which leads to a smoother result.

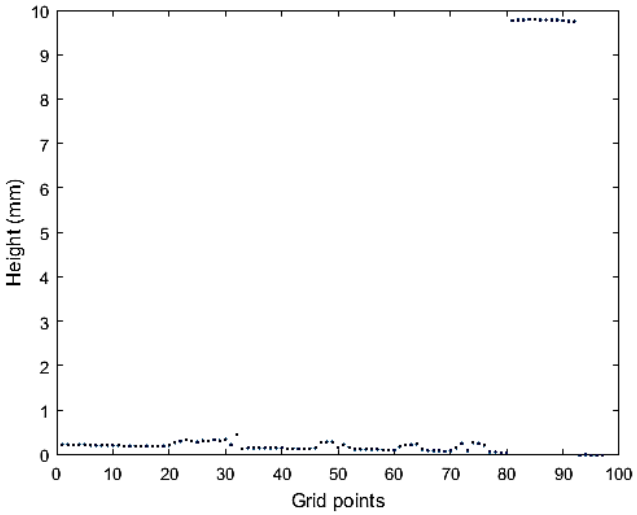

Figure 14: Thickness that was guessed for each grid point, the metal block can be indicated between grid point 80 and 90 on the x axis.

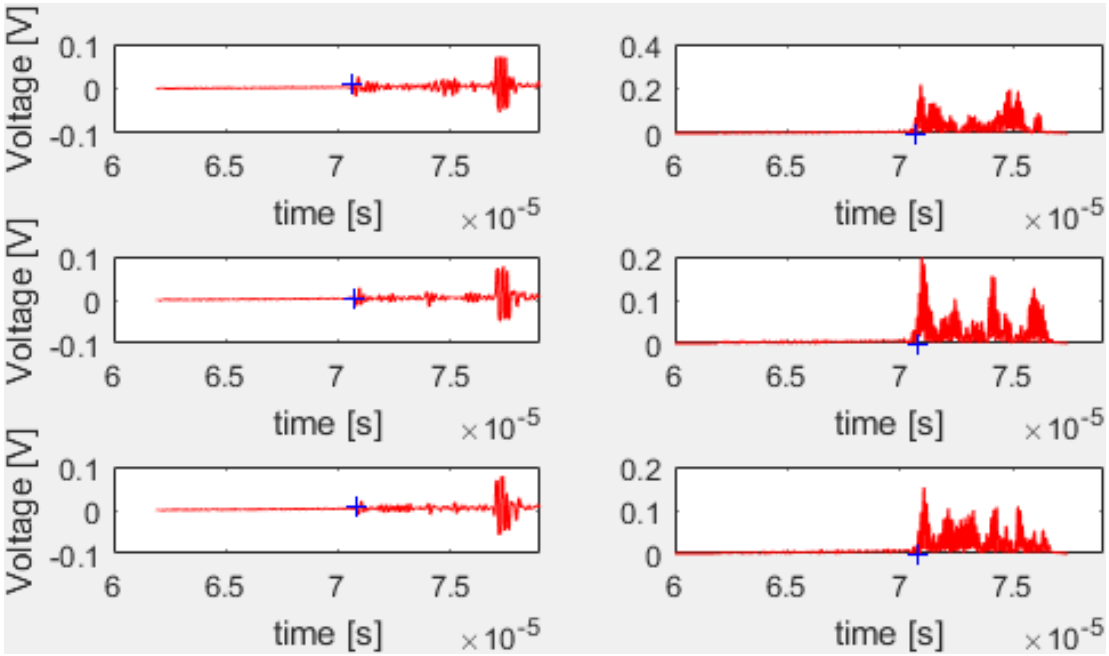

Figure 15: Left: de reflection pulses of the sample indicated by the blue dot (t_1). Right: the cross correlation between the reflection pulse from the sample (t_1) and the reference scan (t_0). The front reflections (t_1) are indicated by the dot in graphs left, the blue dot indicates the point of maximum cross correlation in the right plots.

The thickness ($l(x,y)$) of the sample at each grid point

The thickness ($l(x,y)$) at each grid point was determined with the use of the Matlab script Processingdata_thickness2.m *(Written by Lana Keijzer, Applied Physics, TU Delft, The Netherlands, 2015).* The thickness ($l(x,y)$) at each grid point was determined by Equation 9.

$$l\,(x,y) = \frac{\mathrm{V_{background}}\,(t_0 - t_1(x,y))}{2} \qquad \text{(Equation 9)}$$

The cross correlation between the reference pulse(t_0) and the reflected pulse(t_1) were computed again as presented in (Figure 15). This method was again combined with a method of zero-padding with a factor of 2 in the frequency domain to increase the sampling rate in the time domain which leads to a smoother result.

Because the position of the maximum cross correlation is not at the position of the front reflection in the sample the front reflections (t_1) are localized by selecting the first position were the absolute correlation is 30% of the maximum value of the absolute correlation. This value of 30% was based on trial and error by checking in the peak of the front reflection is selected (Figure 15). This value can differ between samples and were therefore checked for several grid points within each sample and adjusted if needed (Figure 4). For skin and Achilles tendon 30% was sufficient to select the front reflection of the sample.

The thickness (l) was computed (Figure 17). The position of the block is clearly visible on the right side.

Corrected thickness (l)

The errors in the determination of the thickness (l) were filtered by checking the thickness (l) between adjacent points (Figure 17). A threshold of 1 mm difference was set for skin and Achilles tendon. The samples were cut as flat as possible, a bigger difference than 1 mm could indicate for example some fatty tissue that was not removed properly. And even more important a bigger difference between adjacent can indicate that the samples were not positioned completely flat on the

reflector plate. By setting this threshold the edges of the sample are neglected as well. Figure 17 shows the thickness of the samples that are corrected for errors. The sample of Achilles tendon on the right was not used because there were to less data points to use, the sample was not placed correctly on the reflector plate (this was caused by a too weak pumping system).

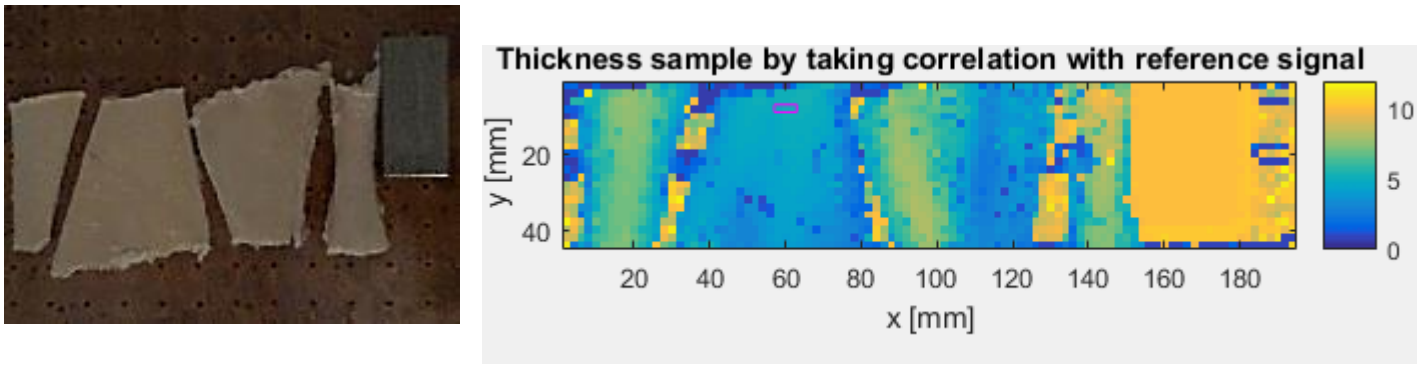

Figure 16: Left: picture of the samples on the reflector plate, right: thickness of the samples in mm.

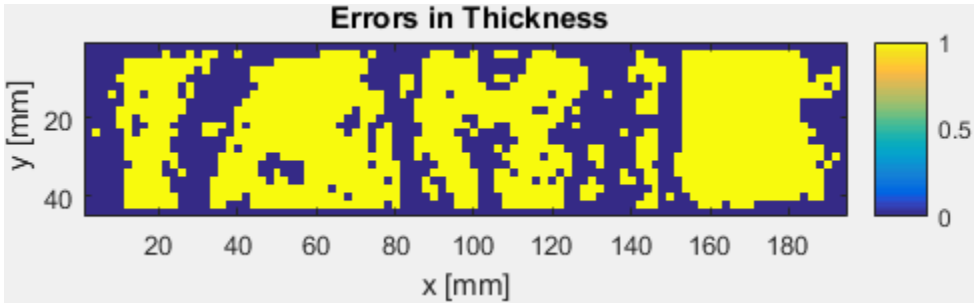

Figure 17 : The thickness in mm corrected for the errors for the four Achilles tendon samples that were placed next to the metal block.

With the use of the plot of the thickness (Figure 17) the area of interest of one specific sample can be selected to compute the average thickness and to compute the longitudinal velocity within each sample. It is important to select the grid points in a way that no parts of the adjacent samples are selected, it is not necessary to select the edges of the samples precisely.

Average thickness

When the sample was selected the thickness corrected for errors was used to compute the mean value.

Longitudinal velocity of the sample (V_{sample})

The longitudinal velocity of the sample ($V_{sample(x,y)}$) was computed for each grid point by Equation 10.

$$V_{sample}(x,y) = \frac{V_{background}(t_0 - t_1(x,y))}{t_2(x,y) - t_1(x,y)} \qquad \text{(Equation 10)}$$

The longitudinal velocity in each sample $(V_{sample}(x,y))$ was determined by the determination of the cross correlation between the reflection pulses (t_0, t_1, t_2) and the reference measurement. Again zero padding with a factor 2 was used to gain a smoother result (Figure 15).

The longitudinal velocity in each sample (V_{sample}) was plotted as in Figure 18. To compute the mean longitudinal velocity in the sample (V_{sample}) first the grid points that were removed in the previous step to determine the thickness of the sample were removed. Second, the range of the longitudinal velocity in the samples (V_{sample}) was chosen based on the top plot in Figure 18 .

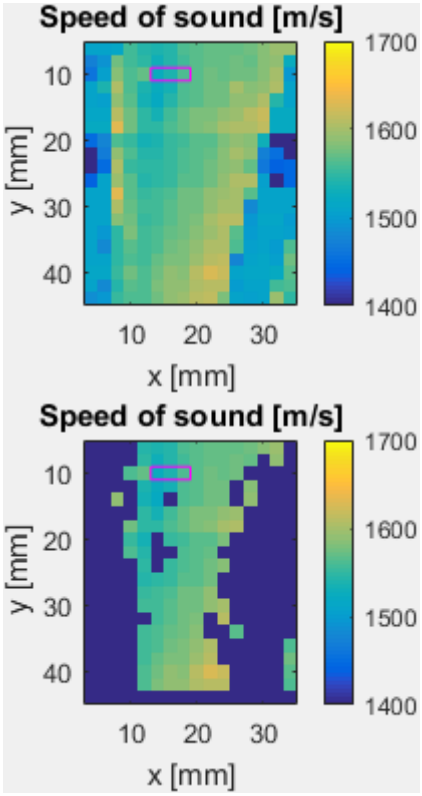

Figure 18 : Longitudinal velocity of the sample (V_{sample}) plotted without correction for errors (top), and corrected for errors (bottom).

Based on the top plot in Figure 18 the range of the longitudinal velocity was selected. The grid points that contain a longitudinal velocity within this range were used to determine the average longitudinal velocity per sample. The selection of this range was computed as an extra check to make sure unexpected outliers were removed, the influences of this extra step is marginal. Several ranges for the longitudinal velocity of the sample were chosen and the mean value was computed as presented in Table 1. This resulted in a mean value of 1567.6 m/s with a standard deviation of 11.54 m/s. The coefficient of variation (ratio of the standard deviation to the mean) within these ranges is 0.7%. This is a marginal coefficient of variation.

Table 10: Range of longitudinal velocity and the average longitudinal velocity

Range of longitudinal velocity of the sample (V_{sample}) chosen based on the top plot in Figure 8. (m/s)	Mean longitudinal velocity in the sample (V_{sample}) (m/s)
1500 - 1600	1564
1525 – 1625	1580

1500 – 1650	1569
1475- 1675	1575

Results for the thickness and longitudinal velocity of Achilles tendon and skin are presented in Table1 (Article) and for the extensor digitorum longus in Table 1 (Appendix D).

Attenuation ($\alpha(x,y)$)

For the data processing of the attenuation (α) of each sample Matlab script 'ProcesData_att2.m 'was used (*Written by Lana Keijzer, Applied physics, TU Delft, The Netherlands, 2015*).
The total attenuation ($\alpha(x,y)$) for each grid point was determined by comparing the Fourier spectrum of the pulse at that grid point to the Fourier spectrum of the reference pulse (Figure 19).

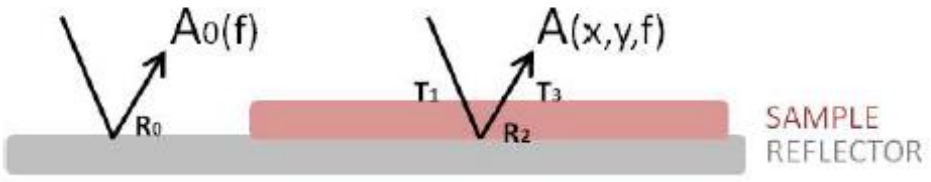

Figure 19 : Fourier transform of the waves that are reflected by the reflector plate ($A_0(f)$) and the sample and the reflector plate (A (x, y, f)) (Image made by Lana Keijzer, Applied physics, TU Delft, The Netherlands, 2015)

The attenuation within the sample was calculated by Equation 11.

$$\alpha(x,y,f) = \frac{-20}{2l}\log_{10}\frac{|A(x,y,f)|}{|A_0(f)|} \qquad \text{(Equation 11)}$$

The computed attenuation was fitted to curves of the following form:

$$\frac{|A(x,y,f)|}{|A_0(f)|} = \alpha_0 \cdot e^{-2af^b l} \qquad \text{(Equation 12)}$$

In this equation a_0 describes the effect caused by transmission and reflection, a is the frequency dependent attenuation coefficient, b is a constant and f represents the frequency.

Selection of the signals

A Tukey window was constructed to select the signals (Figure 20). The Fourier spectra of the signals were taken (Figure 21). The attenuation ($\alpha(x,y)$) was determined for the -6 dB range of the Fourier spectrum of the reference measurement. A least squares fitting was done according to the fitting in Equation 6. The constraints that were imposed were that the variable a and a_0 should be positive and b in the range between 0 and 2 based on literature (2).

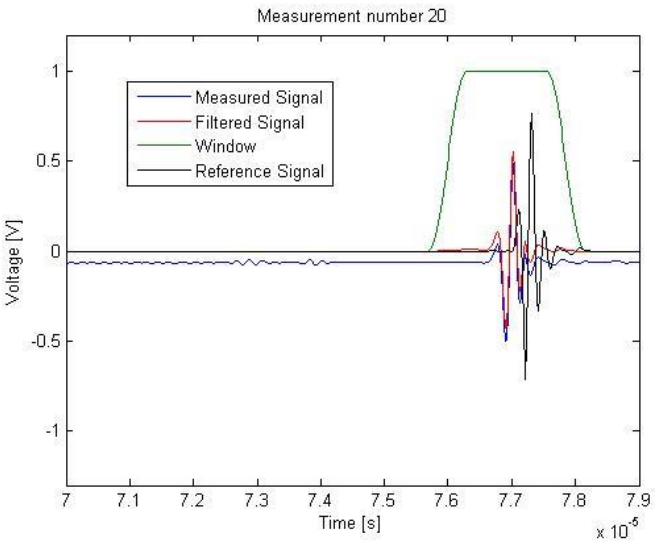

Figure 20: Tukey window that was used to select the signal

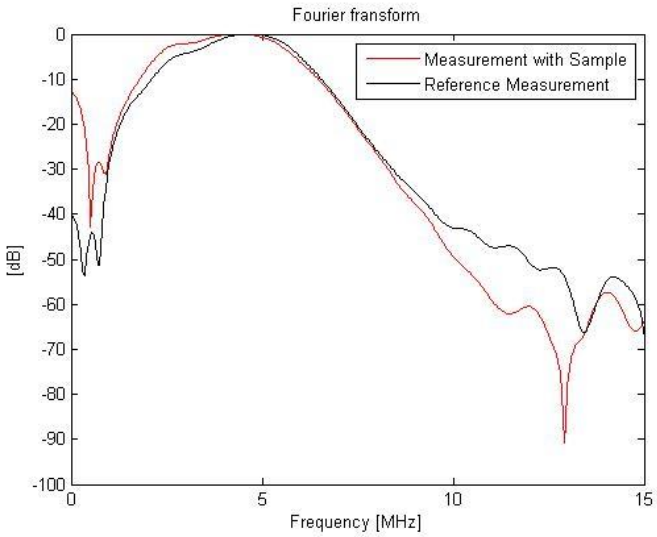

Figure 21 : Fourier spectra of the measurement with sample (blue) and the reference sample (red).

The 3 constants (a, a_0 and b) are plotted and corrected for the errors from the thickness and longitudinal velocity of each sample (Figure 22).

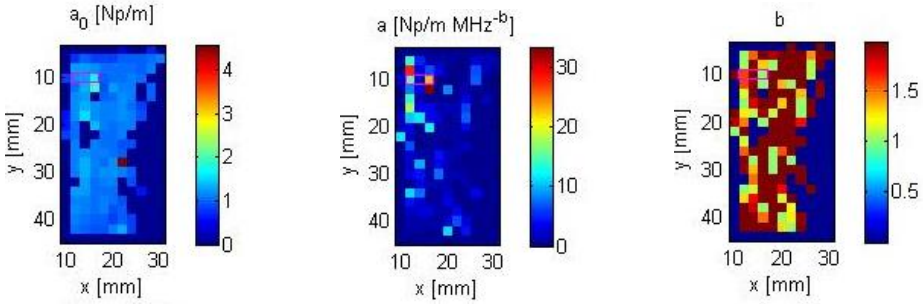

Figure 22: The constants a, a_0 and b corrected for errors in the speed of sound and thickness.

The fitting for three points were plotted so that the fitting could be checked (Figure 23).

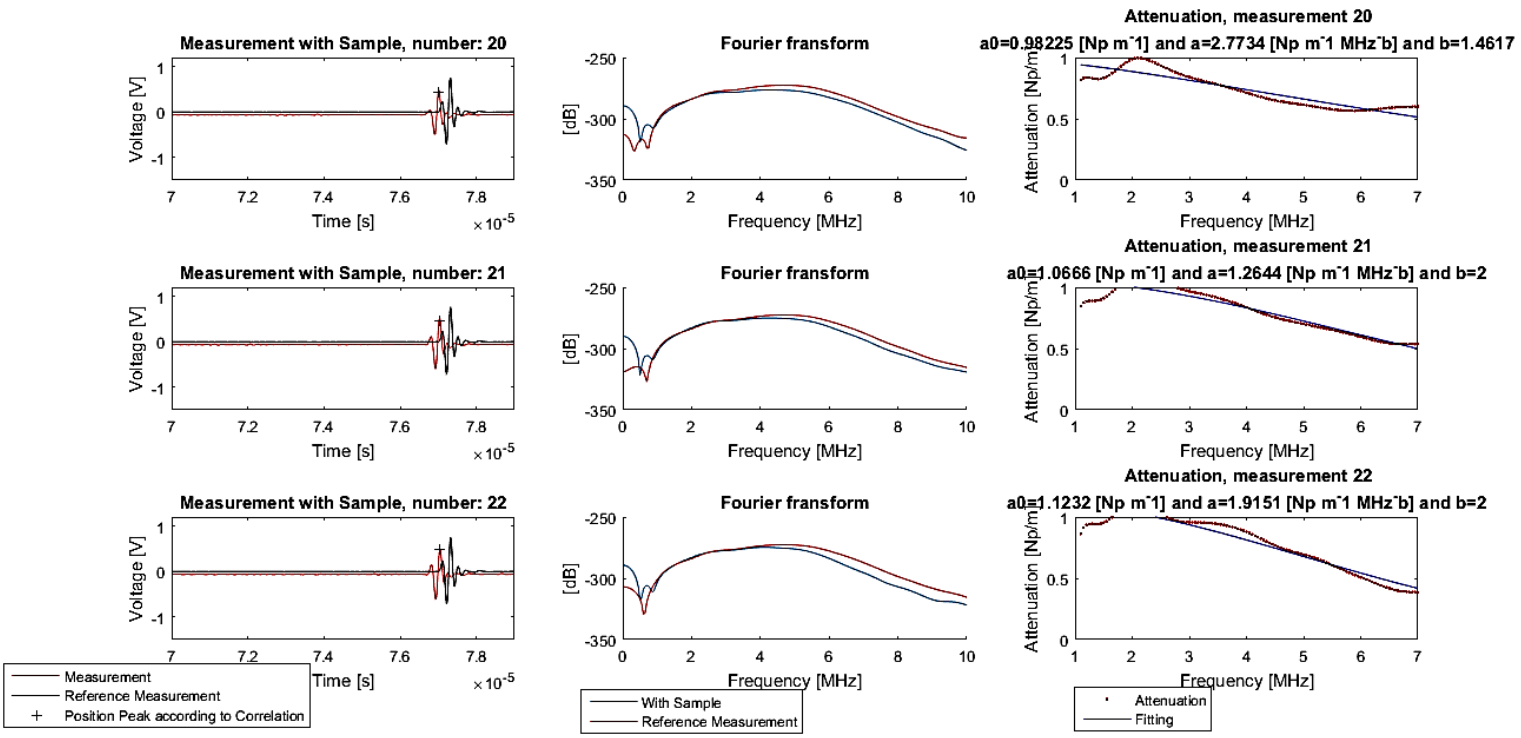

Figure 23: Left: The signals of the signals of the measurements, the reference measurement and the position of the peak according to the correlation. Middle: The Fourier spectra of the measurement and the reference measurement. Right: The fitting of the constants $\boldsymbol{a}$, $\boldsymbol{a}_0$ and b.

Fitting and averaging

The longitudinal velocity within one individual sample (V_{sample}) led to homogenous results whereas the attenuation resulted in a wide variation of variables. Multiple combinations of the fitting constants (a, a_0 and b) can lead to similar fittings. The calculated attenuation was therefore averaged first over all grid points and then the least squared fitting was performed (Figure 22 and Figure 23). Since the sample was assumed to be homogeneous, it is legitimate to keep a single variable constant. By keeping one variable constant, the other variables are also expected to show less variation. The leastsquarees fitting was repeated again for all grid points but the average value voor b was kept constant. The previous step gave the opportunity to remove the outliers of the data easily. When b is kept constant the root mean error (RME) stays similar, whereas if the other constants are kept constant the RME changes. The average fitting values were again determined without the outliers.The mean value for the α, α_0 and b were determined by taking the mean of the values that were obtained by those two fitting steps. Results are presented in Table 1 (Article) and Table 2(Appendix D). The attenuation (a) is presented in dB/cm which was calculated by multiplying the attenuation (a) in Np/m with a factor of 8.686 (2).

Density bottle method

The density of skin and Achilles tendon were determined by the use of the density bottle method as described by DiResta et al.(1990) (3).Two pycnometers (2,17 mL, Fisher Inc, Ottowa, Canada) were used (Figure 24). Each sample was cut into pieces and two measurements per sample were performed. For each individual sample the mean value of the two measurement was computed. A total average value and standard deviation were computed with the mean values of each individual sample per tissue. Phosphate buffered saline (PBS) was used as background medium to mimic in vivo conditions. Measurements were performed at 37℃.

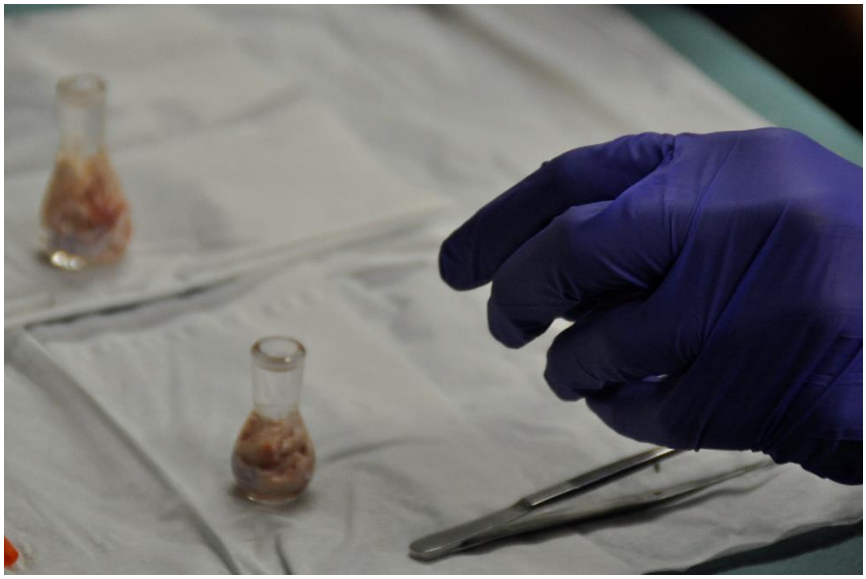

Figure 24 : Pycnometers filled with sample and PBS.

Equation 13 was used for the determination of the density per sample(3):

$$\rho_{sample} = \rho_{pbs} \frac{m_2 - m_1}{m_4 - m_1 - m_3 + m_2} \quad \text{(Equation 13)}$$

1. Weight of the empty pycnometer (m1)
2. Weight of the pycnometer with sample (m2)
3. Weight of the pycnometer with sample and PBS (m3)
4. Weight of the pycnometer with PBS (m4)

A density of 1007 kg/m^3 for PBS was used. Results are presented in Table 1 (Article) and Table 1 (Appendix B).

Recommendations

The Marco scanner requires that the tissues lay completely flat on the reflector plate to encounter planar surfaces. During the current experiment this requirement could not be fulfilled due to a too weak pumping system. Therefore, grid points at which the samples were not directly positioned on the reflector plate were removed before the acoustic parameters were determined. One Achilles tendon sample was discarded because it was not positioned rightly on the reflector plate. For the other samples we had to remove a few grid points per sample, which had marginal effect due to the large number of grid points that we used (approx. 400 grid points per skin sample, and 600 for each Achilles tendon sample). This has led to a decrease in the number of grid points that were used per sample to calculate the longitudinal velocity (V_{sample}), thickness (l) and attenuation (α). For further

research it is recommended to increase the power of the pumping system.

The samples that were used to determine the acoustic parameters were not complete flat, it was challenging to obtain soft tissues with complete flat surface during the dissection step. When the samples are not completely flat, this results in samples without planar surfaces. The assumption of normal incidence does not hold due to the irregularities within the samples which are caused by the dissection step and the inhomogeneous aspects of the human tissues. These irregularities influence the longitudinal velocity less than the frequency dependent attenuation. For calculation of the longitudinal velocity only the phase shift is required.

The large number of grid points per sample (approx. 400 grid points per skin sample, and 600 for each Achilles tendon sample) reduces the influences of above mentioned possible errors (reduction of the number of grid points and deformation of the reflection pulses) at several grid points per sample. The mean values of the longitudinal velocity (V_{sample}), thickness (l) per tissue were found with a small standard deviation. The attenuation (α) resulted in a mean value with a high stand deviation, several reasons are expected to cause this high standard deviation. First, high standard deviations for attenuation were found for skin and bone in literature which subscribes the fact that attenuation is not homogenous within human tissues. Second, the dissection of the tissues has not led to completely flat tissues which leads to a variation in Fourier spectra per grid point. Third, multiple combinations of the fitting constants (a, a_0 and b) can lead to similar fittings.

When the frequency dependent coefficient of tissues for frequencies lower than 1 MHz are required another transducer (with 1 MHz as centre frequency instead of 5 MHz) should be used because the transducer is more accurate around its center frequency.
The bottle density method requires that the air bubbles are completely removed from the pycnometer before the measurements start. Due to the compressibility of soft tissues this was challenging for some samples. This is expected to have caused the larger standard deviation that was found for the density of Achilles tendon.

References

1. Parker KJ. Ultrasonic attenuation and absorption in liver tissue. Ultrasound in medicine & biology. 1983;9(4):363-9.
2. Duck FA. Physical properties of tissues: a comprehensive reference book: Academic press; 2013.
3. DiResta G, Lee J, Lau N, Ali F, Galicich J, Arbit E. Measurement of brain tissue density using pycnometry. Brain Edema VIII: Springer; 1990. p. 34-6.

Appendix D. Acoustic parameters of the extensor digitorum longus and peroneus brevus

The acoustic parameters of the soft tissues present in the ankle joint space are not extensively described by literature. An experiment to determine the density (ρ), thickness (l), acoustic velocity (V_l) and attenuation (α) of the Achilles tendon, skin, extensor digitorum longus and peroneus brevus was therefore conducted (Figure 25). The main interest of our study was on the skin and Achilles tendon, but the acoustic parameters of the extensor digitorum longus and peroneus brevus were determined as well for usage in future studies. The longitudinal velocity, thickness and density of skin and Achilles tendon are reported in Table 1 in the Article.

Figure 25: Samples placed in the macro scanner: left Achilles tendon, middle: Skin, Right: digitorum longus

Specimen

For the experiments tissues from frozen human cadaver ankles were used. The cadaver ankles were defrosted and dissected. The tissue samples were frozen again after dissection and defrosted again a few hours before the experiments. No information about the age or freshness was available.

For the determination of the thickness (l), longitudinal velocity (V_l) and attenuation (α) 6 different cadavers were used. The tissues were collected and cut in to pieces of 5 cm x 5 cm. This resulted in 8 samples of Achilles tendons and 3 skin samples.
For the determination of the density (ρ) 6 other cadaver ankles were used. The following samples were collected: 6 Achilles tendons and 3 skin samples.

For the determination of the of the thickness, longitudinal velocity and attenuation three samples of the extensor digitorum longus from three different cadavers were used. The tissues were collected and cut in to pieces of 5 cm x 5 cm.
For the determination of the density 2 samples of peroneus brevus and 1 sample of an extensor digitorum longus of three different cadaver ankles were used.

Results

The results of the thickness and longitudinal acoustic velocity of the extensor digitorum longus are presented in Table 11 . The attenuation and the fitting constants α_0 and b for skin, Achilles tendon and digitorum longus are presented in Table 12. The density of the peroneus brevus and extensor digitorum longus are presented in Table 3. The longitudinal velocity, thickness and density of Achilles tendon and skin are reported in Table 1 in the Article.

Table 11: The longitudinal acoustic velocity and thickness for the digitorum longus. Values are presented as mean (standard deviation).

Tissue	V_l (m/s)	l (mm)
Extensor digitorum longus	1575(10)	3.3(0.5)

Table 12 : The attenuation and the fitting constants α_0 en b for Achilles tendon, skin and digitorum longus.

	α (Np/m/MHZ)	α_0 (Np/m)	b
Achilles Tendon	8.6	1.2	0.84
	1.3	0.95	2.2
	12	0.92	1.0
	0.22	0.94	2.9
	0.5	0.73	2.4
	0.33	0.87	2.7
	44	2.0	0.40
	47	1.3	0.55
Mean	**14**	**0.93**	**1.6**
Standard deviation	**18**	**0.13**	**0.96**
Skin	12	0.93	1.2
	3.4	0.91	1.9
	14	1.0	1.3
Mean	**10**	**0.96**	**1.5**
Standard deviation	**4.7**	**0.05**	**0.29**
Extensor digitorum Longus	2.0	0.86	1.4
	4.5	0.62	1.2
	5.6	0.84	3.1
Mean	**4.0**	**0.77**	**1.9**
Standard deviation	**1.5**	**0.10**	**0.87**

Table 13: The density for the peroneus brevus and digitorum longus.

	ρ (kg/m^3)
Peroneus brevus	1514
	1513
	1512
	1506
Mean	**1511**
Standard deviation	**3**
Extensor digitorum longus	1511
	1513
Mean	**1512**
Standard deviation	**0.80**

Appendix E. Computational simulations of acoustic wave propagation through the ankle joint space.

Geometry

The geometry of the tibia and talus were based on a CT scan that matched best with a mean shape of a statistical shape model built of the tibia and talus bone based on a database of 72 CT scans of human ankles (Figure 26). The CT images were segmented in Mimics® (Materialise, Leuven, Belgium). The CT-slices on which the talus could be seen ranged from 54.6 until 103.5. Slice 79.05 was taken to create the geometry for the model because it was assumed that this slice showed the ankle joint space in the middle of the ankle. The background of the CT scan was removed with Photoshop. The file was saved as an .PCX file for implementation in the computational model.

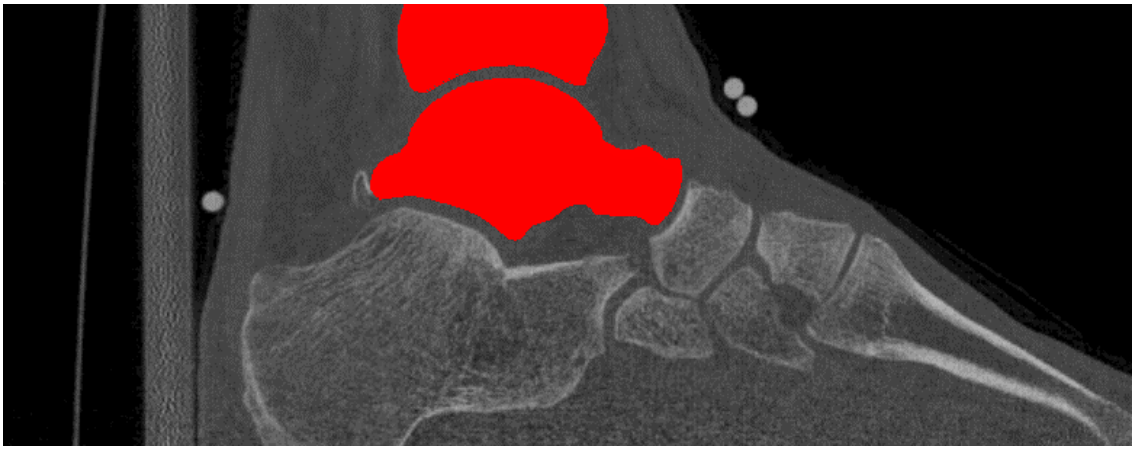

Figure 26 :CT with the segmented talus and tibia that was used to create the geometry of the joint space.

Acoustic wave propagatin through the ankle joint space

Figure 27 shows an graphical reprensentation of acoustic wave propagation through the ankle ankle joint space. It can be clearly seen that a large part of the waves travell through the bones.

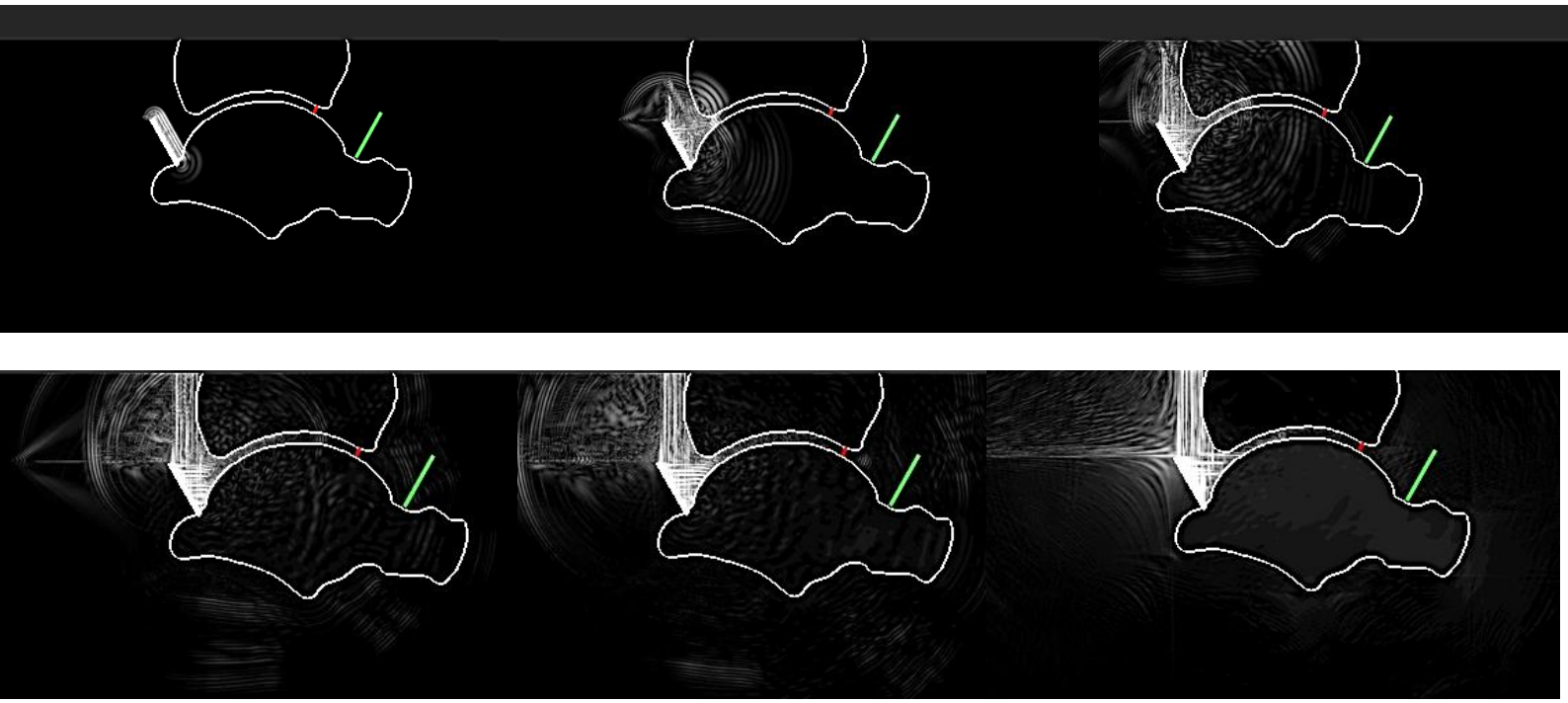

Figure 27: Graphical representation of acoustic wave propagation through the healthy ankle joint space.

Output signals

The output signals of the receiver on the outside of the healthy ankle joint space are represented in Figure 29 – Figure 32.

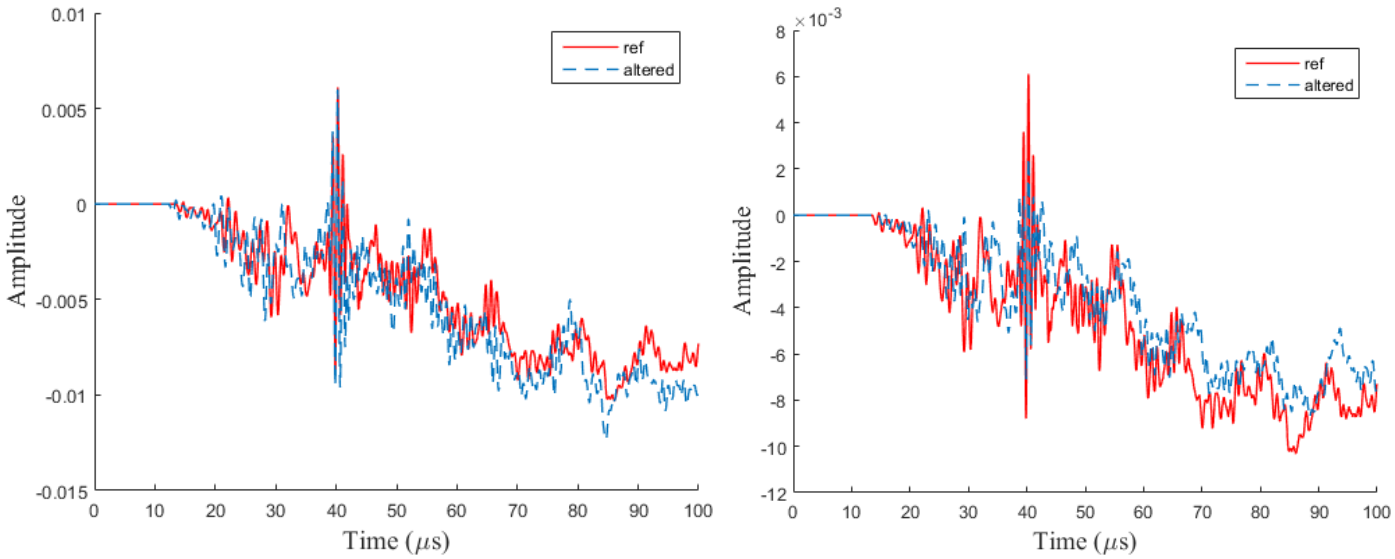

Figure 28 : Output signals of the reference situation (red) and the situation with minimal (left) and maximal (right) density for bone (blue stripes).

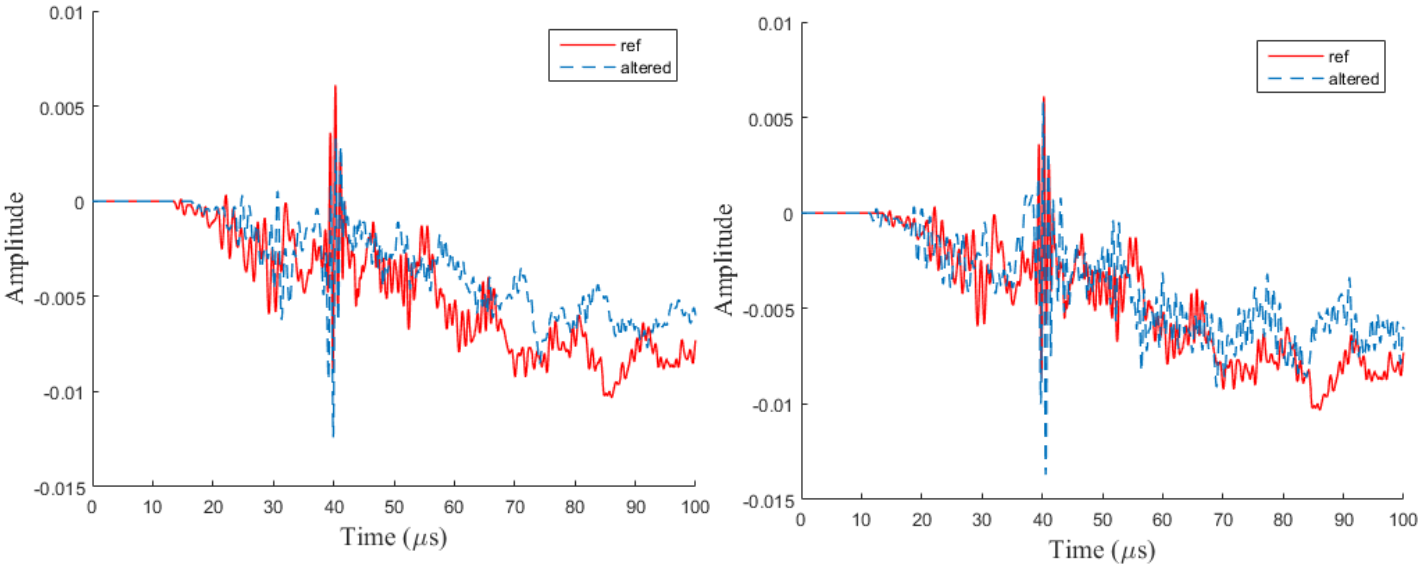

Figure 30: Output signals of the reference situation (red) and the situation with minimal (left) and maximal (right) Lamé's constants for bone (blue stripes).

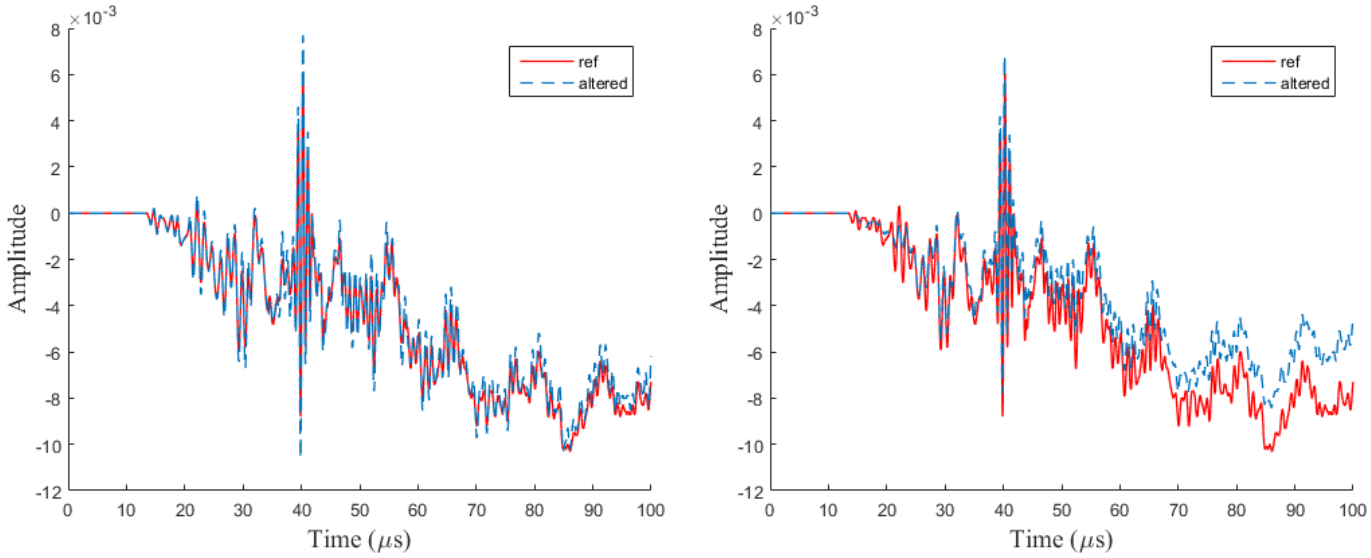

Figure 31: Output signals of the reference situation(red) and the situation with minimal (left) and maximal (right) bulk and shear viscosity for bone (blue stripes).

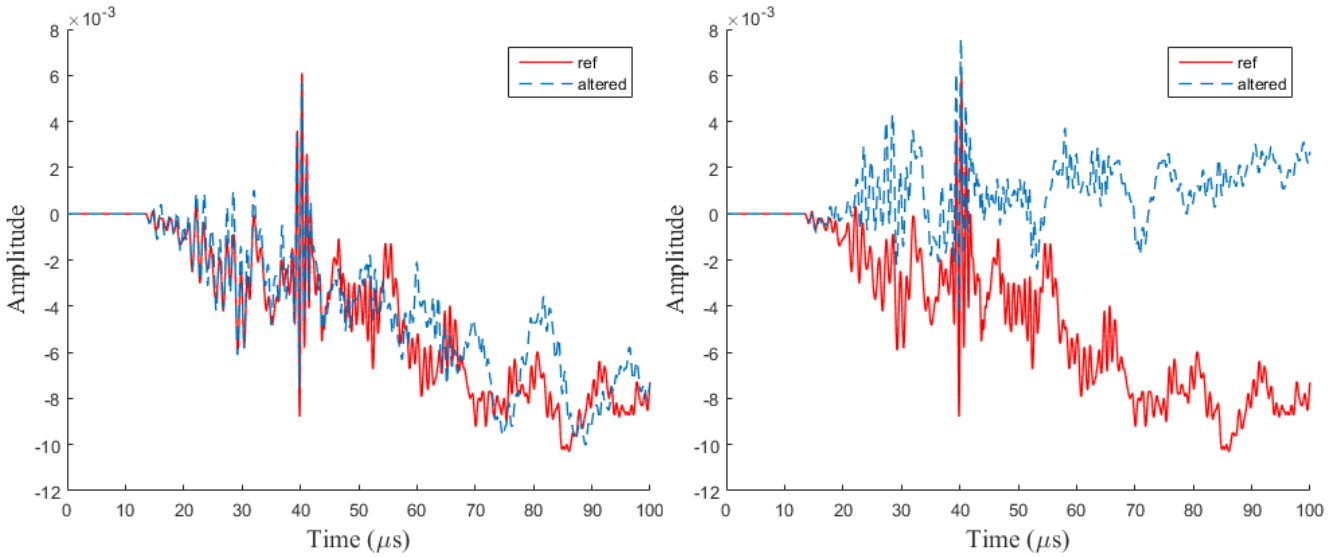

Figure 32: Output signals of the reference situation (red) and situation with the addition on Achilles tendon (left) and Achilles tendon and skin(right) in blue stripes.